

Dimer Models, Free Fermions and Super Quantum Mechanics

Robbert Dijkgraaf^{1,2}, Domenico Orlando³ and Susanne Reffert¹

¹ *Institute for Theoretical Physics, University of Amsterdam, Valckenierstraat 65, 1018XE Amsterdam, The Netherlands.*

² *KdV Institute for Mathematics, University of Amsterdam, Plantage Muidergracht 24, 1018 TV Amsterdam, The Netherlands.*

³ *Università di Milano-Bicocca and INFN, Sezione di Milano-Bicocca, P.zza della Scienza, 3, I-20126 Milano, Italy*

ABSTRACT

This note relates topics in statistical mechanics, graph theory and combinatorics, lattice quantum field theory, super quantum mechanics and string theory. We give a precise relation between the dimer model on a graph embedded on a torus and the massless free Majorana fermion living on the same lattice. A loop expansion of the fermion determinant is performed, where the loops turn out to be compositions of two perfect matchings. These loop states are sorted into co-chain groups using categorification techniques similar to the ones used for categorifying knot polynomials. The Euler characteristic of the resulting co-chain complex recovers the Newton polynomial of the dimer model. We re-interpret this system as supersymmetric quantum mechanics, where configurations with vanishing net winding number form the ground states. Finally, we make use of the quiver gauge theory – dimer model correspondence to obtain an interpretation of the loops in terms of the physics of D -branes probing a toric Calabi–Yau singularity.

Contents

1	Introduction	2
2	Dimer Model Preliminaries	4
3	The dimer model as a free fermion	7
3.1	The Dirac operator and the Kasteleyn matrix	7
3.2	The scaling limit	10
3.3	The loop expansion of the fermion determinant	11
3.4	Loops as fermionic states	15
4	Categorification of the Newton polynomial	18
4.1	The dimer model on the cylinder and supersymmetric QM	20
4.2	Example: One square on the cylinder	23
4.3	Loops as operators	24
4.4	The dimer model on the torus and supersymmetric QM	26
5	Gauge theory interpretation: Preliminaries	30
5.1	The quiver gauge theory	31
5.2	Exceptional collections and helices	32
5.3	The correspondence	33
6	Gauge theory interpretation: Results	34
6.1	Matchings and acyclic quivers	36
6.2	Seiberg dualities and graph isomorphisms	38
6.3	Interpretation of the $(0,0)$ -loops	40
6.3.1	Plaque moves	40
6.3.2	Relation to crystal melting and black holes	40
6.4	Interpretation of the loops with non-trivial winding	41
7	Conclusions	42
A	Perfect matchings in the operator formalism	45
B	Generating functions	47
B.1	Generating function for the fermion loops on the cylinder	47
B.2	Generating function for the fermion loops on the torus	47
C	Example: One square on the torus	48

1 Introduction

The dimer model is concerned with the statistical mechanics of close packed dimer arrangements on a bipartite graph. The physical system which can be thought of as a real world representation of the dimer model is the adsorption of diatomic molecules on a crystal surface.

In the 1960s, the question of how many perfect matchings exist on a plane graph was solved independently by Kasteleyn [1, 2], and Temperley and Fisher [3, 4]: the total number is given by the Pfaffian of a signed, weighted adjacency matrix of the graph (the Kasteleyn matrix). Much of the original interest in the dimer model arose because it provides a simple and elegant solution for the 2-dimensional Ising model [5].

The problem of enumerating perfect matchings is of course a classical problem in graph theory and combinatorics, see *e.g.* [6]. It can also be phrased in terms of domino tilings [7]. During the last years, the interest in the dimer model was revived thanks its manifold connections to other branches of mathematics and physics. The dimer model is related to

- configurations of a melting crystal corner and the topological string A-model [8, 9],
- real algebraic geometry [10, 11],
- BPS black holes from D -branes wrapping collapsed cycles [12].

Furthermore, a correspondence between the dimer model and quiver gauge theories arising from $D3$ -branes probing a singular toric surface was discovered and worked out in great detail [13, 14, 15, 16, 17]. An explanation of this correspondence via mirror symmetry was given in [18].

That the dimer model must be related to the free massless fermion on the same lattice has been known for a long time already. Its relation to the Ising model, which in turn corresponds to a free fermion model clearly indicates this. Moreover, Kasteleyn also showed that the partition function of the dimer model living on a graph embeddable on a genus g Riemann surface is given by a linear combination of 2^{2g} Pfaffians. This is, of course, reminiscent of the number of spin structures on a Riemann surface. In fact, a one-to-one correspondence between equivalence classes of Kasteleyn orientations and spin structures was proved in [19].

In the following, we will make the connection between the dimer model and the free fermion precise by identifying the Dirac operator with the Kasteleyn matrix and relating the expansion of the determinant appearing in the free fermion path integral to loop configurations composed of two perfect matchings. This picture of free fermions as a loop gas already appeared in a different context, for example in [20].

The perfect matchings form a basis for the space of fermion loop configurations. If the loop gas lives on a surface of non-trivial homotopy, non-contractible loops of non-zero

winding number can occur, and the Pfaffian of the Kasteleyn matrix becomes a polynomial. Drawing inspiration from the categorification programme of Khovanov [21, 22, 23], we interpret this polynomial as the Euler characteristic of a co-chain complex. The loop configurations of the free fermion model can be naturally classified by the weight of the constituent matchings of the loop state and used to generate Abelian groups. For the Euler characteristic to coincide with the Newton polynomial, a differential operator must be constructed accordingly. In our fermion loop gas, all loop states are paired since they come in two opposite orientations, except for states consisting only of double line perfect matchings. This is reminiscent of the supersymmetric ground states in supersymmetric quantum mechanics. Indeed, it is possible to re-interpret the fermion loop gas as SQM and to construct a differential operator which can be identified with the Q operator. Like this, the Newton polynomial becomes the generalized Witten index of the system. Since the fermion loop states are bilinear in the perfect matchings, they can also be interpreted as maps from one matching to another.

Thanks to the correspondence between the dimer model and quiver gauge theory, we know that the perfect matchings, *i.e.* our zero modes, parametrize the toric surface being probed by the D -branes. In the following, we make use of this correspondence to give the loops states an interpretation in terms of the quiver gauge theory. Loops of vanishing net winding can be related to sequences of double Seiberg dualities on the associated acyclic quivers. In the special case of the hexagon graph, they correspond to certain BPS black hole configurations which are parametrized by melting crystal configurations [12].

The plan of this paper is as follows. In Section 2, we review the necessary background and definitions of the dimer model. In Section 3.1, we relate the Kasteleyn matrix to the discretized Dirac operator of the free fermion. In Section 3.2, we go to the limit of vanishing lattice spacing in which we recover the partition function of the Dirac fermion, which in the light of the interpretation of the dimer model as a free fermion model is no longer surprising. In Section 3.3, we expand the determinant arising in the free fermion path integral into cyclic permutations, which correspond to closed loops on the graph. Furthermore, we give an interpretation of the loops as fermionic states in Subsection 3.4.

In Section 4, the basic idea of categorification is explained, and in Section 4.1, the fermion loop system is re-interpreted as supersymmetric quantum mechanics. The simpler case of a square graph on the cylinder is worked out first, together with a simple explicit example in Section 4.2. In Section 4.3, we interpret the loops as operators mapping from one perfect matching to another. Finally, Section 4.4 gives the full construction on the torus.

In Section 5, the basics of quiver gauge theories and the correspondence to the dimer model is reviewed. The interpretation of the loop states in terms of the physics of D -branes probing a singular toric CY is attempted in Section 6. In Section 6.1, the relation between perfect matchings and corresponding acyclic quiver graphs is clarified. In Section 6.2, we

show that sequences of double Seiberg dualities correspond to cyclic permutations of the nodes of the acyclic quiver and to isomorphisms of the full gauge quiver. With these results, we can interpret the loops with vanishing overall winding in Section 6.3. The loops with non-trivial winding are discussed in Section 6.4.

The results of this paper are summarized in a dictionary given in Section 7, where we close with some concluding remarks.

2 Dimer Model Preliminaries

Take a plane *bipartite* graph \mathcal{G} , *i.e.* one in which all vertices can be colored black and white, such that each black vertex is only connected by links to white vertices and vice versa. Let M be a subset of the set E of edges of \mathcal{G} . M is called a *matching*, if its elements are links and no two of them are adjacent. If every vertex of \mathcal{G} is saturated under M , the matching is called *perfect*. Such a link which joins a black and a white vertex is also called a *dimer*. The dimer model describes the statistical mechanics of a system of random perfect matchings. In the simplest case, we ask for the number of close packed dimer configurations, *i.e.* the number of perfect matchings.

Let us label the vertices of the underlying graph \mathcal{G} on which the dimer model lives consecutively. The topology of \mathcal{G} can be encoded in its adjacency matrix A , where $A_{x,y} = 1$ if the vertices x and y are joined by an edge, and $A_{x,y} = 0$ otherwise. The number of perfect matchings is given by the number of ways in which the vertices can be partitioned into adjacent pairs.

The *Hafnian* of a symmetric matrix A , introduced by Caianiello [24], is defined as

$$\text{Hf}(A) = \sum_{\pi \in \mathcal{S}} A_{\pi(1),\pi(2)} A_{\pi(3),\pi(4)} \cdots A_{\pi(n-1),\pi(n)}, \quad (1)$$

where \mathcal{S} is the set of all permutations π of $\{1, \dots, n\}$ satisfying $\pi(1) < \pi(3) < \dots < \pi(n-1)$ and $\pi(2i-1) < \pi(2i)$ for $1 \leq i \leq n/2$, n even. If we take A to be the adjacency matrix of \mathcal{G} , $\text{Hf}(A)$ counts the perfect matchings, since terms in (1) which contain non-adjacent pairs are zero. The *permanent* of an $n \times n$ matrix A is, like the determinant, given by the sum over all permutations, except that the sign of the permutations is not taken into account:

$$\text{perm}(A) = \sum_{\pi \in S_n} \prod_{i=1}^n A_{i,\pi(i)}. \quad (2)$$

While the determinant can be evaluated in polynomial time via Gaussian elimination, computing the permanent is $\#P$ -complete [25]. The Hafnian can be regarded as a generalization

of the permanent. In fact [26],

$$\text{Hf}(A) = \text{perm}(B) \text{ for } A \text{ of the form } A = \left(\begin{array}{c|c} 0 & B \\ \hline B^t & 0 \end{array} \right). \quad (3)$$

This identity accounts for the fact that sometimes, the number of perfect matchings is given as the permanent of the adjacency matrix in the literature. Like the permanent, also the Hafnian is difficult to evaluate and does not satisfy any useful identities.

The counterparts of the Hafnian and permanent are the *Pfaffian* and determinant, which take into account the sign of the permutations:

$$\text{Pf}(A) = \sum_{\pi \in \mathcal{S}} \text{sign}(\pi) A_{\pi(1),\pi(2)} A_{\pi(3),\pi(4)} \cdots A_{\pi(n-1),\pi(n)}, \quad (4)$$

$$\det(A) = \sum_{\pi \in \mathcal{S}_n} \text{sign}(\pi) \prod_{i=1}^n A_{i,\pi(i)}, \quad (5)$$

where the permutations contributing to the Pfaffian are subject to the same conditions as for the Hafnian. Here, we have

$$\text{Pf}(A') = (-1)^{\binom{n}{2}} \det(B) \text{ for } A' \text{ of the form } A' = \left(\begin{array}{c|c} 0 & B \\ \hline -B^t & 0 \end{array} \right). \quad (6)$$

Moreover, for every anti-symmetric matrix of even order, the relation

$$\det A = (\text{Pf } A)^2 \quad (7)$$

holds. Already in 1913, Polya suggested to change some signs in a matrix A , such that the determinant of the new matrix \tilde{A} would be the permanent of A [27]. Kasteleyn [1, 2] actually does exactly this: he introduces an orientation on \mathcal{G} , which leads to a signed adjacency matrix K , now called the *Kasteleyn matrix*. The Pfaffian of K gives the number of perfect matchings.

A *Kasteleyn orientation* fulfills the following condition: the product of all edge weights around a face must equal -1 if the number of edges around the face is $0 \pmod{4}$. If the number of edges equals $2 \pmod{4}$, the product must equal 1 [6]. One can choose an orientation by consistently assigning arrows to the edges of the graph, as originally suggested by Kasteleyn [1, 2]. For our purposes, it turns out to be more convenient to allow the roots of 1 as (complex) edge weights.

Already Caianiello [24] remarked that the expectation value of any product of free Fermi fields is a Pfaffian, while the expectation value of any product of free Bose fields is a Hafnian. In this sense Kasteleyn's method of attaching signs to the edges of a graph \mathcal{G} could be seen as a fermionization of a bosonic system. Given the correspondence of the dimer model to

the free fermion on \mathcal{G} , one could look for its bosonic equivalent, but this goes beyond the scope of the present work.

In the following, we will consider graphs embedded on a cylinder or a torus. The treatment can be straightforwardly generalized to any genus g Riemann surface. In essence, all of the above remains true. The only change is that on the torus (cylinder), we have two (one) non-trivial cycles, which we will denote by z and w . In the case of the plane graph, the edge weights originated solely from the Kasteleyn orientation. More generally, the Kuperberg flatness condition must be respected [28]. We choose a positive direction on the dimers, say $\bullet \rightarrow \circ$. Now we assign the weight z (w) to each edge which crosses the cycle z (w) in positive direction and the weight $1/z$ ($1/w$) to each edge which crosses it in negative direction. While the Pfaffian of the Kasteleyn matrix yielded a number in the case of the plane graph, it now becomes a polynomial in z and w , the so-called characteristic polynomial or *Newton polynomial* of the graph. The coefficient of each monomial $z^p w^q$ gives the number of matchings with *weight* $(z, w) = (p, q)$. These are matchings with the number of dimers crossing z in positive direction minus the number of dimers crossing z in negative direction equal to p (analogous for q). In the literature, what we call the weight is usually referred to as the slope of a height function defined on the composition of two matchings. The height function is defined as follows. Choose a reference matching PM_0 . To find the slope of a matching PM , compose it with the reference matching, $\text{PM} - \text{PM}_0$, where the minus serves to change the orientation of PM_0 to $\circ \rightarrow \bullet$. This results in closed loops (composition cycles) and double line dimers. The rule is that when an edge in PM belonging to a closed loop is crossed such that the black node is to its left (right), the height changes by $+1$ (-1). If an edge belonging to PM_0 is crossed, the signs are reversed. This height function is defined up to the choice of the reference matching PM_0 . Crossing the boundary of the fundamental region of the torus, this function can jump. If the height function jumps by p units crossing z , it is associated to the power z^p in the Newton polynomial of the graph (and equivalently for w). Choosing a different reference matching results in a common prefactor of $z^{p_0} w^{q_0}$ for all monomials. Our method of assigning weights to a matching corresponds to choosing a reference matching of weight $(0, 0)$ that does not intersect the z or w cycle. The matching shown in Figure 1 has weight $(1, 0)$, where $1 = 2 - 1$.

The characteristic, or Newton polynomial, of the dimer model on the torus takes the form

$$P(z, w) = \sum_{n_z, n_w} N_{n_z, n_w} (-1)^{n_z + n_w + n_z n_w} z^{n_z} w^{n_w}, \quad (8)$$

where the N_{n_z, n_w} count the number of matchings that have weight (height change) (n_z, n_w) . Furthermore, the partition function which counts the total number of matchings for the

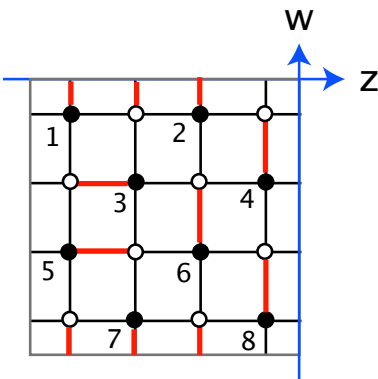


Figure 1: Example of a square graph on the torus

square graph on the torus is given by

$$Z = \frac{1}{2} (-P(1,1) + P(1,-1) + P(-1,1) + P(-1,-1)), \quad (9)$$

where the first term is always zero. $P(z,w)$ evaluated in $z,w = \pm 1$ corresponds to the contributions of the four different spin structures.

3 The dimer model as a free fermion

As already mentioned in the introduction, many clues point towards the equivalence of the dimer model and the free fermion living on the same lattice. On one hand, we know that the dimer model corresponds to the two-dimensional Ising model. In the continuum limit, the critical Ising model corresponds in turn to the free Majorana fermion. Another clue is that the partition function of the dimer model on a genus g Riemann surface is a linear combination of 2^{2g} Pfaffians, one for each of the different boundary conditions. The one-to-one correspondence between the 2^{2g} equivalence classes of Kasteleyn orientations and the spin structures was proved in [19].

Note that our construction given in the following is different from the transfer matrix approach used in [29, 30, 31].

3.1 The Dirac operator and the Kasteleyn matrix

In this section, we show that the dimer model on a square lattice can be naturally mapped to the dynamics of a free massless fermion on the same lattice. More precisely, we will see how introducing a Kasteleyn orientation on the graph can be thought of as the projection of the ∂ operator on γ matrices, see also [32, 6].

Let us consider the theory for a free massless fermion on a bipartite square graph¹. At this stage, the construction is independent of the boundary conditions, *i.e.* we can think of the model as living on the infinite plane. The graph being bipartite, it is natural to use staggered fermions [35] and associate a two–component real spinor to each pair of nodes:

$$\Psi = \begin{pmatrix} \chi_{\bullet} \\ \chi_{\circ} \end{pmatrix}. \quad (10)$$

The naive discretization of the free massless fermion action becomes then

$$S = \int d x \bar{\Psi}(x) \not{\partial} \Psi(x) = \sum_{\langle x, y \rangle} \chi(x) \not{\partial}(x, y) \chi(y), \quad (11)$$

where the sum runs over all neighbouring vertices x and y on the lattice. The discretized Dirac operator can be cast into the form

$$\not{\partial}(x, y) = \gamma^{\mu} \frac{x_{\mu} - y_{\mu}}{|x - y|}, \quad (12)$$

where γ^{μ} are two matrices satisfying the Clifford algebra $\{ \gamma^{\mu}, \gamma^{\nu} \} = 2 \delta^{\mu\nu}$ in two Euclidean dimensions. On the square lattice, each node has four neighbours, separated by unit vectors, so the action reads

$$S = \sum_{x \in E(\mathcal{G})} \sum_{k=1}^4 \chi(x) \gamma^{\mu} e^k_{\mu} \chi(x + e^k), \quad (13)$$

where e^k is the vector $e^k = (\cos \frac{2k\pi}{4}, \sin \frac{2k\pi}{4})$. If x is a \bullet site, $x \pm e^k$ is a \circ site and vice versa. This means that we can split the action into two pieces:

$$S = \left(\vec{\chi}_{\bullet} \mid \vec{\chi}_{\circ} \right) \begin{pmatrix} 0 & \not{\partial}_{\bullet\circ} \\ \not{\partial}_{\circ\bullet} & 0 \end{pmatrix} \begin{pmatrix} \vec{\chi}_{\bullet} \\ \vec{\chi}_{\circ} \end{pmatrix} = \vec{\chi}_{\bullet} \cdot \not{\partial}_{\bullet\circ} \cdot \vec{\chi}_{\circ} + \vec{\chi}_{\circ} \cdot \not{\partial}_{\circ\bullet} \cdot \vec{\chi}_{\bullet}, \quad (14)$$

where $\vec{\chi}_{\bullet}$ is the vector of Grassmanian variables living on the \bullet nodes. Let us consider the first term. The operator $\not{\partial}_{\bullet\circ}$ is non–vanishing if and only if \bullet and \circ are neighbours, and takes values proportional to the components of the γ matrices. More precisely, if we think of $\not{\partial}_{\bullet\circ}$ as a matrix, each line will contain four non–vanishing entries $\{ \gamma^1_{\bullet\circ}, \gamma^2_{\bullet\circ}, -\gamma^1_{\circ\bullet}, -\gamma^2_{\circ\bullet} \}$. Choosing the representation

$$\gamma^1 = \begin{pmatrix} 0 & 1 \\ 1 & 0 \end{pmatrix}, \quad \gamma^2 = \begin{pmatrix} 0 & i \\ -i & 0 \end{pmatrix}, \quad (15)$$

these components read $\{ 1, i, -1, -i \}$. These are the weights of the four links around each \bullet

¹A different definition for the Dirac operator, such as the one given in [33, 34] would be needed to deal with a general random graph. This goes beyond the scope of the present note.

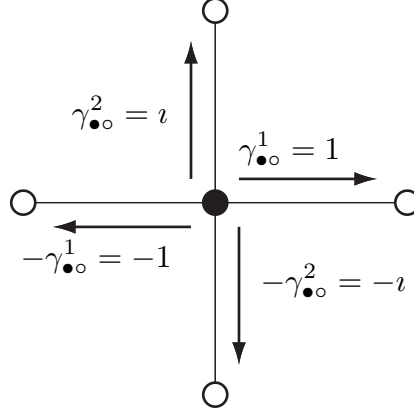


Figure 2: Dirac operator

node. Since their product equals to (-1) and on this graph the product of weights around a node is the same as the product around a plaquette, this is precisely a Kasteleyn orientation (see Fig. 2)²

The same construction can of course be repeated for the second term in Eq. (14). In this case, we get for each line of the operator $\partial_{\circ\bullet}$ the four non-vanishing elements $\{\gamma_{\circ\bullet}^1, \gamma_{\circ\bullet}^2, -\gamma_{\circ\bullet}^1, -\gamma_{\circ\bullet}^2\}$ which, in the same representation for the γ matrices that we used above, read $\{1, -i, -1, i\}$, yielding again a Kasteleyn orientation.

Adjacency matrices with equivalent Kasteleyn orientations have the same determinant (up to an overall sign), therefore we have

$$\det(\partial_{\bullet\circ}) = \det(\partial_{\circ\bullet}) = \text{Pf}(K), \quad (16)$$

where K is a Kasteleyn matrix for the graph. Writing the partition function for the free massless fermion gives

$$Z_{\text{fermion}} = \int \mathbf{d}\psi e^{-S[\psi]} = \sqrt{\det(\partial)} = \sqrt{\det(\partial_{\bullet\circ}) \det(\partial_{\circ\bullet})} = \text{Pf}(K), \quad (17)$$

which is precisely the number of perfect matchings on the lattice for a given boundary condition.

Explicit expressions for both the dimer model on a square graph and the free fermion

²This argument can be easily generalized to any regular tessellation of the hyperbolic plane (leading to higher-genus graphs). One can show that for an n -gon, the product of the weights around a node is (-1) if $n = 0 \pmod{4}$ and $(+1)$ if $n = 2 \pmod{4}$. For the hexagonal lattice (genus one), the weights around a \bullet site read $\{1, e^{2\pi i/3}, e^{-2\pi i/3}\}$ and their product is $(+1)$. It is worth to remark that for higher genus surfaces, there is no unique global choice of complex structure.

theory are known. Take a triangular lattice describing a torus with periodicity

$$z = z + iN + jMe^{i\theta}, \quad i, j \in \mathbb{Z}, z \in \mathbb{C}, \quad (18)$$

i.e. with modular parameter $\tau = \frac{M}{N}e^{i\theta}$. In [36], it is shown that the partition function for a vortex with winding (a, b) on this lattice, which can be mapped to a free fermion, is given by the infinite product

$$Z_{\text{vortex}}^{[a]}(M, N, \theta) = \prod_{k=-M/2}^{M/2} \prod_{l=-N/2}^{N/2} 2 \left| \alpha \cos \left(2\pi \frac{k}{M} + \pi \frac{a}{M} \right) + \beta \cos \left(2\pi \frac{l}{N} + \pi \frac{b}{N} \right) + \gamma \cos \left(2\pi \left(\frac{k}{M} - \frac{l}{N} \right) + \pi \left(\frac{a}{M} - \frac{b}{N} \right) \right) - \sigma \right|, \quad (19)$$

where

$$\alpha = \beta = \frac{1 - \cos \theta}{\sin^2 \theta}, \quad \gamma = \frac{\cos \theta}{\sin^2 \theta}, \quad \sigma = \frac{2 - \cos \theta}{\sin^2 \theta}. \quad (20)$$

Specializing this formula for a square torus with $\theta = \pi/2$ such that $\alpha = \beta = 1, \gamma = 0, \sigma = 2$, we find:

$$Z_{\text{vortex}}^{[a]}(M, N, \frac{\pi}{2}) = \prod_{k=-M/2}^{M/2} \prod_{l=-N/2}^{N/2} 2 \left| \cos \left(\frac{2k\pi}{M} + a \frac{\pi}{M} \right) + \cos \left(\frac{2l\pi}{N} + b \frac{\pi}{N} \right) - 2 \right|, \quad (21)$$

which is precisely the partition function of the dimer model.

3.2 The scaling limit

Having shown that the dimer model on a graph is equivalent to a free Majorana fermion theory, we expect the torus partition function to be modular invariant in the thermodynamical limit, and to consist of theta functions.

Since this is a universal property, we specialize to a particular lattice, for example the $M \times N$ square graph. The partition function for this model was discussed in [2, 7] and takes the form

$$Z_{MN} = \frac{1}{2} \sum_{a,b=0}^1 (-1)^{a+b+ab} Z_{MN}^{[a]}, \quad (22)$$

where

$$Z_{MN}^{[a]} = \prod_{k=-M/2}^{M/2} \prod_{l=-N/2}^{N/2} 2 \left| \cos \left(\frac{2k\pi}{M} + a \frac{\pi}{M} \right) + \cos \left(\frac{2l\pi}{N} + b \frac{\pi}{N} \right) - 2 \right|. \quad (23)$$

If we regard the $M \times N$ lattice as a discretization of a square torus with modular parameter

$\tau = it$ into $M \times N$ squares, the scaling limit is obtained by taking

$$M, N \rightarrow \infty \quad \frac{M}{N} = t, \quad t \text{ fixed.} \quad (24)$$

This corresponds to sending the lattice size $\frac{1}{M}$ to zero.

As we have previously pointed out, this is precisely the same expression found for a soliton on a triangular lattice [37]. After a careful analysis, the authors prove that in the continuum limit, this reproduces the Ray–Singer result for the $\bar{\delta}$ -torsion of the torus [38] (see also [39, 40]):

$$Z_{MN}^{[a]} \xrightarrow[\substack{M, N \rightarrow \infty \\ M/N = -i\tau}]{} \left[\frac{\vartheta_{[b]}^{[a]}(\tau)}{\eta(\tau)} \right]^2. \quad (25)$$

Instead of reproducing the proof, we will limit ourselves here to a heuristic argument. In the infrared limit, the cosine can be approximated by a parabola and the functions above behave as follows:

$$\begin{aligned} Z_{MN}^{[a]} &= \prod_{k=-M/2}^{M/2} \prod_{l=-N/2}^{N/2} 2 \left| \cos \left(\frac{2k\pi}{M} + a \frac{\pi}{M} \right) + \cos \left(\frac{2l\pi}{N} + b \frac{\pi}{N} \right) - 2 \right| \sim \\ &\sim \prod_{k=-M/2}^{M/2} \prod_{l=-N/2}^{N/2} \frac{8\pi^2}{M^2} \left| \left(k + \frac{a}{2} \right)^2 + \left(l + \frac{b}{2} \right)^2 t^2 \right|. \end{aligned} \quad (26)$$

In the ζ -function regularization, one recognizes the usual product expansion for the theta functions. More precisely, introducing $\tau = it$ we find

$$Z_{MN}^{[a]} \xrightarrow[\substack{M, N \rightarrow \infty \\ M/N = -i\tau}]{} \left[\prod_{k \in \mathbb{Z}} \prod_{l \in \mathbb{Z}} \left| k + \frac{a}{2} + \left(l + \frac{b}{2} \right) \tau \right| \right]^2 = \left[\frac{\vartheta_{[b]}^{[a]}(\tau)}{\eta(\tau)} \right]^2, \quad (27)$$

$$Z_{MN} = \frac{1}{2} \sum_{a,b=0}^1 (-1)^{a+b+ab} Z_{MN}^{[a]} \xrightarrow[\substack{m, n \rightarrow \infty \\ m/n = -i\tau}]{} \frac{1}{2} \sum_{a,b=0}^1 (-1)^{a+b+ab} \left[\frac{\vartheta_{[b]}^{[a]}(\tau)}{\eta(\tau)} \right]^2 = Z_{\text{Dirac}}(\tau). \quad (28)$$

The final result is that in the scaling limit, the partition function is the one of a Dirac fermion, or equivalently, for two Majorana fermions. It is not surprising that we encounter a fermion doubling effect [41, 42] since we have started with a periodic dispersion relation.

3.3 The loop expansion of the fermion determinant

After having shown the equivalence of the discretized Dirac operator and the Kasteleyn orientations and the appearance of the Dirac fermion partition function in the scaling limit, we will now directly relate the dimer model to the free fermion via a diagrammatic expansion of the fermion determinant.

Consider a Grassmanian field χ living on the nodes $V(\mathcal{G})$ of a graph \mathcal{G} described by a

quadratic action:

$$S[\Psi] = \sum_{x,y \in V(\mathcal{G})} \chi_x A_{x,y} \chi_y. \quad (29)$$

As we have seen in Eq. (10), we can associate a two-component Majorana fermion $\Psi = \begin{pmatrix} \chi_\bullet \\ \chi_\circ \end{pmatrix}$ to each black–white pair in a bipartite graph. The path integral for such an action is easily computed and is given by the Pfaffian of the matrix A :

$$Z_{\text{fermion}} = \int \left[\prod_{x \in V(\mathcal{G})} d\chi_x \right] e^{\frac{1}{2} \vec{\chi} A \vec{\chi}} = \text{Pf}(A), \quad (30)$$

where $\vec{\chi}$ is the vector $\vec{\chi} = \{\chi_1, \chi_2, \dots, \chi_{|V(\mathcal{G})|}\}$. In fact, expanding the exponential (and using the fact that χ_x are Grassmanian variables), we find:

$$Z_{\text{fermion}} = \int \left[\prod_{x \in V(\mathcal{G})} d\chi_x \right] \prod_{x < y} (1 - \chi_x A_{x,y} \chi_y). \quad (31)$$

All the factors in the product commute, therefore we can order them by increasing x . Expanding, the terms that survive the integration are those which contain each variable exactly once, hence they are products of the $|V(\mathcal{G})|/2$ matrix elements $A_{x,y}$. There is one such product for each of the permutations of the nodes. Taking into account the signs, we recover the expression for the Pfaffian in Eq. (4).

In the following, we give a diagrammatic expansion for the partition function in terms of loops on the graph. Instead of the Pfaffian, we can thanks to relation (7) expand the determinant under the square root. By definition, the determinant is a sum over all possible permutations π of the lattice points, see Eq. (5). The signature $\text{sign}(\pi)$ of a permutation is easily found by expressing π as the composition of cyclic permutations:

$$\pi = \pi_s \circ \pi_{s-1} \circ \dots \circ \pi_l \circ \dots \circ \pi_1, \quad (32)$$

where π_l is a cyclic permutation of l_r elements. We define

$$\text{sign}(\pi_l) = (-1)^{l_r+1} \quad (33)$$

and

$$\text{sign}(\pi) = \prod_{l=1}^s \text{sign}(\pi_l). \quad (34)$$

Each cyclic permutation π_l can be represented by a closed loop in the graph by joining the vertex x by a directed line to the point $\pi_l(x)$, see *e.g.* [20]. Each vertex in $V(\mathcal{G})$ can be:

- isolated if the permutation does not act on it;
- joined to another one by a double line if the permutation interchanges the two;

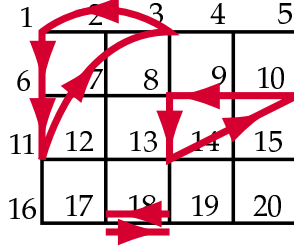


Figure 3: The diagrammatic representation for the permutation $\pi = \pi_3 \circ \pi_2 \circ \pi_1$ with $\pi_1 : (17, 18) \mapsto (18, 17)$, $\pi_2 : (8, 9, 10, 13) \mapsto (9, 10, 13, 8)$ and $\pi_3 : (1, 3, 11, 6) \mapsto (3, 11, 6, 1)$.

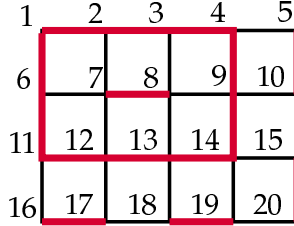


Figure 4: The diagrammatic representation for a permutation allowed by the action for a free massless fermion. Orientations are not represented.

- joined to two others as part of a cyclic chain.

In particular, a permutation of two neighbouring points is a dimer (with a double line).

A general permutation π is represented by a graph obtained as the disjoint union of such loops, and the determinant is written as the weighted sum of all possible such graphs. Note that two points can be joined by a line even if they are not neighbouring on the lattice. If we do not impose further constraints on the form of the matrix A , we have a sum over all the $|V(\mathcal{G})|!$ possible permutations and the general term *will not* be a subgraph of \mathcal{G} (see Fig. 3).

A given graph only contributes to the determinant if the product of the $A_{x\pi(x)}$ along its edges is non-vanishing. This means that imposing constraints on the form of A reduces the number of terms needed.

- A is a *local* operator if $A_{x,y} = 0$ when x and y are not neighbouring. In this case, the only loops contributing to the determinant are those constructed as unions of edges in $E(\mathcal{G})$, and we can limit ourselves to summing over subgraphs of \mathcal{G} .
- If A does not allow self-interactions, *i.e.* $A_{x,x} = 0, \forall x \in V(\mathcal{G})$, we can consider only permutations such that $\pi(x) \neq x, \forall x \in V(\mathcal{G})$. Diagrammatically, this means that we only consider subgraphs without isolated points.

The Dirac operator on the graph in Eq. (12) enjoys both properties. In other words, when representing the path integral for massless free fermions diagrammatically, we consider all

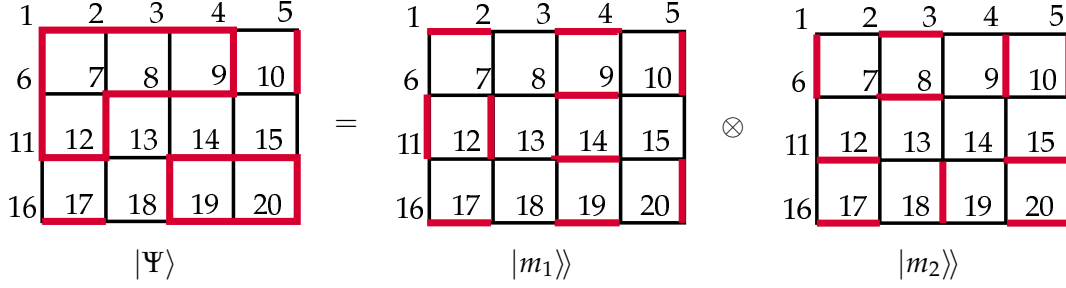


Figure 5: Decomposition of a subgraph $|\Psi\rangle$ containing two loops as the combination $|\Psi\rangle = |m_1\rangle \otimes |m_2\rangle$. Orientations are not represented.

subgraphs containing all the vertices, composed of closed loops or dimers, and without any isolated points. An example of such a configuration is depicted in Fig. 4.

On a bipartite graph, each of these contributing loop configurations can be seen as the composition of two perfect matchings. This decomposition is indeed unique. Let $|m_i\rangle$ and $|m_j\rangle$ be two perfect matchings. We define the combination $|\Psi\rangle = |m_i\rangle \otimes |m_j\rangle$ as the collection of all dimers belonging to either of the matchings, taken with the usual $\bullet \rightarrow \circ$ orientation if the edge is in $|m_i\rangle$ and with the opposite one if it is in $|m_j\rangle$. Any subgraph $|\Psi\rangle$ contributing to the determinant can always be written in this way. In fact:

- if $|\Psi\rangle$ does not contain any loops, its edges are in one-to-one correspondence with those of a perfect matching $|m\rangle$ and we define $|\Psi\rangle \doteq |m\rangle = |m\rangle \otimes |m\rangle$;
- if $|\Psi\rangle$ contains one loop, this loop consists of an even number of edges since the graph is bipartite. Therefore we can decompose it into two disjoint sets of edges that join all the vertices. It follows that we can always find two matchings $|m_i\rangle$ and $|m_j\rangle$ that only differ by a shift by one dimer on the loop and are equal on all the isolated dimers in $|\Psi\rangle$. Note that the state $|\tilde{\Psi}\rangle$ containing the same loop with reversed orientation corresponds simply to $|\tilde{\Psi}\rangle = |m_j\rangle \otimes |m_i\rangle$;
- if $|\Psi\rangle$ contains n loops (which we regard here as unoriented), it can be constructed as the composition of any of the perfect matchings containing the disjoint sets of dimers making up each loop. It is easy to convince oneself that there are 2^n such combinations, corresponding to the 2^n possible orientations of the loops (see Fig. 5).

Note that the composition of two perfect matchings always generates an allowed configuration. In fact, in each of the matchings, every point in $V(\mathcal{G})$ is touched by an edge and in the resulting subgraph, each point is either reached by two distinct lines (and then is part of a loop) or by a double one (and is part of a dimer).

If on a graph \mathcal{G} , there are k perfect matchings, the determinant is written as the sum over k^2 subgraphs.

3.4 Loops as fermionic states

As we have seen in the last section, the partition function for the free fermion can be expanded as a sum over loop configurations on the lattice. Here we show how these configurations can be understood in terms of fermionic states.

Consider a square graph on the torus with N horizontal and M vertical cells, each identified by a vector $\mathbf{z} = (z, w) = z \mathbf{e}_1 + w \mathbf{e}_2$. Let $h(\mathbf{z})$ be the height function defined on a loop configuration. The function can be labelled by two integers p, q , corresponding to the following periodicity conditions:

$$h_{p,q}(\mathbf{z} + n_1 N \mathbf{e}_1 + n_2 M \mathbf{e}_2) = h_{p,q}(\mathbf{z}) + n_1 p + n_2 q, \quad \forall n_i \in \mathbb{Z}. \quad (35)$$

The integers (p, q) are clearly the winding numbers for the loop configuration.³

We would like to consider one of the two coordinates (say z) as Euclidean time and hence see the system as the description of a fermion in $1 + 1$ Euclidean dimensions. To each plaquette we associate the operators $a(\mathbf{z}), a^\dagger(\mathbf{z}), b(\mathbf{z}), b^\dagger(\mathbf{z})$ living on the left edge, with the following interpretations. The operator $a^\dagger(\mathbf{z})$ creates a particle at point w for all times $z' \geq z$ and raises the height function by 1 on the right of point \mathbf{z} , while the operator $b^\dagger(\mathbf{z})$ creates an antiparticle at point \mathbf{z} and lowers the height function by 1 on the right. We impose the usual anticommutation relations

$$\{a(\mathbf{z}), a^\dagger(\mathbf{z}')\} = \delta_{\mathbf{z}, \mathbf{z}'}, \quad \{b(\mathbf{z}), b^\dagger(\mathbf{z}')\} = \delta_{\mathbf{z}, \mathbf{z}'}, \quad (37)$$

all the other anticommutators vanishing. In particular, we recover the constraint $(a^\dagger)^2 = (b^\dagger)^2 = 0$, which can be translated to the fact that the height function cannot jump by more than one unit when passing to an adjacent plaquette. As usual, one can construct a highest-weight representation for the algebra by introducing a state $|0\rangle$ which is annihilated by all the a and b

$$a(\mathbf{z}) |0\rangle = b(\mathbf{z}) |0\rangle = 0, \quad (38)$$

and defining a general state as the result of the action of a sequence of a^\dagger and b^\dagger on $|0\rangle$:

$$|\Psi\rangle = b^\dagger(\mathbf{z}_1) \dots b^\dagger(\mathbf{z}_{N_b}) a^\dagger(\mathbf{z}_{N_b+1}) \dots a^\dagger(\mathbf{z}_{N_b+N_a}) |0\rangle. \quad (39)$$

³One can define a consistent wavefunction for a \mathbb{Z}_k parafermion as

$$\psi_{p,q}^{(k)}(\mathbf{z}) = e^{\frac{2\pi i}{k} h(\mathbf{z})}. \quad (36)$$

Here, we concentrate on the $k = 2$ fermionic case, but the formalism can be extended easily.

is equivalent to requiring that on any allowed state $|\Psi\rangle$:

$$h(z, w) |\Psi\rangle = \left[\sum_{\zeta=0}^z N_a(\zeta, w) - N_b(\zeta, w) \right] |\Psi\rangle = \left[\sum_{\omega=0}^w N_c(z, \omega) - N_d(z, \omega) \right] |\Psi\rangle, \quad (43)$$

where by allowed we mean that it contributes to the Berezin integral.

Note that $h(\mathbf{z}) |0\rangle = 0$, and since the operator $a^\dagger(\mathbf{z}) b^\dagger(\mathbf{z})$ anticommutes with $h(\mathbf{z})$, one can easily see that an allowed state $|\Psi\rangle$ corresponds to a perfect matching if and only if it is annihilated by $h(\mathbf{z})$:

$$h(\mathbf{z}) |PM\rangle = 0. \quad (44)$$

Other interesting operators can be defined:

$$H_z |\Psi\rangle = [h(N, \bar{w}) - h(0, \bar{w})] |\Psi\rangle = \left[\sum_{\zeta=1}^N N_a(\zeta, \bar{w}) - N_b(\zeta, \bar{w}) \right] |\Psi\rangle, \quad (45a)$$

$$H_w |\Psi\rangle = [h(\bar{z}, M) - h(\bar{z}, 0)] |\Psi\rangle = \left[\sum_{\omega=1}^M N_c(\bar{z}, \omega) - N_d(\bar{z}, \omega) \right] |\Psi\rangle, \quad (45b)$$

where \bar{w} (resp. \bar{z}) is an arbitrary value. Note that both operators are global since they are defined for the whole graph and do not depend on the choice of \bar{z} or \bar{w} . We can consider $h(\mathbf{z})$ as their local counterpart. H_z, H_w count the winding numbers of a state $|\Psi\rangle$ in the z and w directions:

$$H_z |\Psi_{p,q}\rangle = p |\Psi_{p,q}\rangle, \quad (46a)$$

$$H_w |\Psi_{p,q}\rangle = q |\Psi_{p,q}\rangle. \quad (46b)$$

In particular, states with vanishing winding numbers will be annihilated by both H_z and H_w . Another operator is the one that interchanges each a^\dagger with a b^\dagger , each c^\dagger with a d^\dagger and viceversa:

$$Q_1 |\Psi\rangle = \prod_{\mathbf{z}} \left[a^\dagger(\mathbf{z}) b(\mathbf{z}) + b^\dagger(\mathbf{z}) a(\mathbf{z}) \right] \left[c^\dagger(\mathbf{z}) d(\mathbf{z}) + d^\dagger(\mathbf{z}) c(\mathbf{z}) \right] |\Psi\rangle. \quad (47)$$

One can easily verify that $\{Q_1, h(\mathbf{z})\} = 0$. It follows that Q_1 leaves the perfect matchings invariant and pairs all the other states such that $Q_1 |\Psi_{p,q}\rangle = |\tilde{\Psi}_{p,q}\rangle = |\Psi_{-p,-q}\rangle$.

A diagrammatic representation for a general state $|\Psi\rangle$ is easily obtained as follows. For each operator $a^\dagger(\mathbf{z})$, one adds a vertical upward arrow on the left edge of the plaquette at point \mathbf{z} , for each $b^\dagger(\mathbf{z})$ a downward arrow on the left edge of the plaquette, for each $c^\dagger(\mathbf{z})$ a left pointing arrow on the bottom of the plaquette and for each $d^\dagger(\mathbf{z})$ a right pointing arrow on the bottom of the plaquette (see Fig. 7).

In Sec. 3.3, we found the loop states to be combinations of two perfect matchings. We can

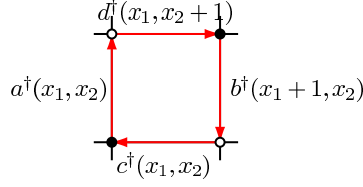


Figure 7: Diagrammatic representation for the four creation operators around a plaquette with coordinates (z, w) .

indeed recover the same result in terms of this operator formalism, see Appendix A for the details, where we also give a necessary and sufficient condition for a state $|\Psi\rangle$ to be allowed.

Let us summarize the contents of this rather technical section. The terms contributing to the expansion of the path integral in Eq. (17) can be represented as resulting from the action of a set of operators $a^\dagger, b^\dagger, c^\dagger$ and d^\dagger , defined on the lattice, on a vacuum $|0\rangle$. This set is redundant in the sense that the knowledge of the a^\dagger and b^\dagger operators, plus the consistency conditions in Eq. (111) uniquely identifies the c^\dagger and d^\dagger .

We interpret the two directions in the graph as a Euclidean time (z) and a space coordinate (w). The operator $a^\dagger(z, w)$ creates a particle at time z and position w that propagates at the same position for all times $z \leq z' \leq N$. In the same way, $b^\dagger(z, w)$ creates an antiparticle. The height function $h(z, w)$ computes the local charge (+1 for particles and -1 for antiparticles) at point w and time z . The charge gradient H_w between the points $w = 0$ and $w = M$ at fixed time \bar{z} is conserved during the time evolution. A loop configuration with winding numbers (H_z, H_w) represents the time evolution of a system with initial charge gradient H_w , whose net charge in any fixed point in space \bar{w} jumps by H_z between $z = 0$ and $z = N$. In particular, a $(0, H_w)$ loop describes a time evolution where no net charge is created globally, while a perfect matching corresponds to a system where no net charge is present at the initial time nor is created locally.

4 Categorification of the Newton polynomial

What follows is inspired by the categorification programme for knot polynomials of Khovanov [21, 22, 23]. The basic idea of his work is that for a knot K , a doubly graded homology theory $H_{i,j}(K)$ can be constructed, whose graded Euler characteristic with respect to one of the gradings yields the knot polynomial in question, e.g. the Jones polynomial, or the Alexander polynomial. The homology groups are constructed through a categorification process which starts with a state sum representation of the invariant polynomial. A group is constructed for each term in the summation, and differential maps between these groups are appropriately defined. Similar categorifications were subsequently performed for other invariants with state sums, e.g. various graph polynomials, such as the chromatic poly-

mial [43, 44], and the more general Tutte polynomial [45].

But exactly what is meant by the term categorification? When we categorify, we replace set theoretic concepts by category theoretic ones. Sets become categories, functions become functors, and equations between functions become natural isomorphisms between functors (fulfilling certain relations). The opposite process, decategorification, is much more familiar to us. When we decategorify, we are basically throwing away extra information by taking all isomorphic objects to be equal. When we say that all vector spaces of the same dimension are the same, we decategorify and are left with a set of isomorphism classes. Obviously, the reverse process of inventing the missing information is much more difficult. The category FinSet of all finite sets for example is a categorification of the set of natural numbers. For an easy to read introduction to the concept of categorification, we refer the reader to [46].

After this general digression, we return to our own system of fermion loops. Its partition function, the Newton polynomial, is, once more, a state sum. From the point of view of the dimer model, its integer coefficients and polynomial nature are obvious. From the point of view of the free fermion, this is much less so. Giving this partition function the interpretation of a graded Euler characteristic explains its integer nature and gives it a geometric interpretation, while at the same time suggesting its relation to an index.

The task at hand is obvious: construct a bigraded co-chain complex from the fermion loop states with a differential map preserving the grading, such that the Euler characteristic of this co-chain complex yields the Newton polynomial.

The fact that we can associate four different charges to each loop state living on the torus (see Eq. (112)) gives us a certain freedom in the choice of the gradings in the double complex. Our emphasis is placed on the matchings, so we choose to sort the loop states into co-chain groups according to the maximum winding number of the two constituent matchings in one direction ($\max_i H_p |m_i\rangle\rangle$) and to define an internal grading based on the maximum weight in the other direction ($\max_i H_q |m_i\rangle\rangle$). This seemingly arbitrary choice just amounts to picking a horizontal and a vertical direction in the double complex. The Euler characteristic, for example, is not sensitive to this choice.

When studying the loop states, there is an obvious observation to make: because of the two possible orientations of the loops, all states are paired with the exception of the double line perfect matchings. This very much smells of supersymmetric Quantum mechanics (SQM), where the supersymmetric ground states are the only ones which need not be paired. Indeed, if one takes the total weight of a configuration to be its energy, the perfect matchings, having zero winding, become ground states.

The Witten index,

$$\dim \mathcal{H}_{(0)}^B - \dim \mathcal{H}_{(0)}^F = \text{Tr}(-1)^F, \quad (48)$$

counts the number of bosonic minus fermionic ground states and is an invariant of the sys-

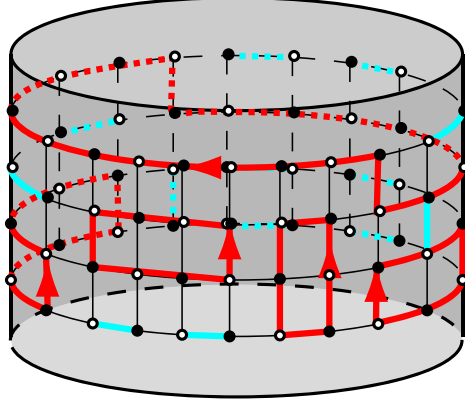


Figure 8: A loop configuration on the cylinder. In red: closed loops; in blue: double lines. This configuration has winding number $k - l = +1$

tem. This is, indeed, also what the Newton polynomial is doing! Once we re-interpret our fermion loop gas as a SQM system and construct a co-chain complex such that its boundary operator can be identified with the Q operator and states with opposite orientations become superpartners, the partition function becomes the generalized Witten index of the system.

This will be done explicitly in the following sections.

4.1 The dimer model on the cylinder and supersymmetric QM

In this section, we show how to construct a co-chain complex out of the loop configurations of a free fermion on a lattice, and how this system can be mapped to a SQM system in which the loop configurations correspond to pure states. For simplicity, we first confine ourselves to a square graph embedded on a cylinder where only one non-trivial cycle is present. A typical example of such a loop configuration is represented in Figure 8.

We have seen in Section 3.3 that a loop configuration can always be decomposed into a superposition of two matchings. Let us introduce the following notation:

- a matching with weight k is written as $|k, a\rangle$, where $a = 1, \dots, N_k$ labels the matchings of the same weight;
- we label a loop as $|k, a; l, b\rangle_\epsilon$ with $k \geq l$, $\epsilon = \pm 1$. This corresponds to one of the following combinations of matchings:

$$\begin{aligned}
 |k, a; l, b\rangle_+ &= |k, a\rangle \otimes |l, b\rangle && \text{if } k > l, \\
 |k, a; l, b\rangle_- &= |l, b\rangle \otimes |k, a\rangle && \text{if } k > l, \\
 |k, a; k, b\rangle_+ &= |k, a\rangle \otimes |k, b\rangle && \text{if } a > b, \\
 |k, a; k, b\rangle_- &= |k, b\rangle \otimes |k, a\rangle && \text{if } a > b, \\
 |k, a; k, a\rangle_+ &= |k, a\rangle \otimes |k, a\rangle, \\
 |k, a; k, a\rangle_- &= 0.
 \end{aligned} \tag{49}$$

Opposite polarizations ϵ correspond to opposite orientations of the same loop configuration. States of the type $|k, a; k, a\rangle_+$ (which are in one-to-one correspondence with the perfect matchings) are singled out because they are not paired.

Since each loop configuration with a given orientation can be uniquely decomposed into matchings, these quantum numbers can be assigned to a given configuration by inspection. The weight of a matching is given by the number of dimers crossing the boundary of the fundamental region in positive direction minus the number of dimers crossing the boundary of the fundamental region in negative direction (where we choose $\bullet \rightarrow \circ$ as orientation). $\epsilon(k-l)$ is the total winding number of the loop configuration (which coincides with the slope of the height function as defined in Sec. 2). States of the type $|k, a; k, a\rangle$ are in one-to-one correspondence with the perfect matchings. All other states are paired (i.e. there are two polarizations). From now on, we will omit to specify the degeneracy quantum numbers and write a loop as $|k; l\rangle_\epsilon$ (note the semicolon).

The quantum numbers can be seen as eigenvalues for the following operators:

$$H |k; l\rangle_\epsilon = (k-l) |k; l\rangle_\epsilon , \quad (50)$$

$$K |k; l\rangle_\epsilon = k |k; l\rangle_\epsilon , \quad (51)$$

$$\Pi |k; l\rangle_\epsilon = \epsilon |k; l\rangle_\epsilon . \quad (52)$$

They commute on the above loop configurations by definition. It follows that H (which we want to identify with the energy) commutes also with the operator

$$F = 2K - \frac{1}{2} (\Pi - 1) , \quad (53)$$

which we identify with the fermion number operator.

In terms of the loops, the above operators have the following interpretation. H counts the (unsigned) total winding number of the state. K counts the maximum attainable total monodromy of a loop configuration. The state $|k; l\rangle_\epsilon$ allows for maximally k overall (i.e. positively minus negatively oriented) homologically non-trivial windings, of which $k-l$ are actually realized. If H is identified with the energy, k gives the maximum possible energy. Each loop with non-trivial winding which is added to the configuration raises the energy of the state by one unit. Ground states do not contain non-contractible loops. The matchings, in particular, contain no loops at all. The eigenvalue of the polarization operator Π is the sign of the winding number. The fermion number operator F is constructed such, that positive polarization states $|k; l\rangle_+$ have even fermion number $2k$, while the fermion number of the corresponding negative polarization states $|k; l\rangle_-$ is raised by one, i.e. is $2k+1$. The operator $(-1)^F$ gives a \mathbb{Z}_2 grading according to the fermion parity. States with positive polarization have even parity, while states negative polarization have odd parity.

To obtain the structure of a SQM, we need to construct two conserved supercharges Q and Q^\dagger which satisfy the following algebra (see *e.g.* Chapter 10 of [47]):

$$\{Q, Q\} = 0 \qquad \{Q^\dagger, Q^\dagger\} = 0 \qquad (54)$$

$$\{Q, Q^\dagger\} = 2H \qquad (55)$$

$$[F, Q] = Q \qquad [F, Q^\dagger] = -Q^\dagger. \qquad (56)$$

A possible choice is the following:

$$\begin{cases} Q |k; l\rangle_+ = \sqrt{2(k-l)} |k; l\rangle_-, \\ Q |k; l\rangle_- = 0. \end{cases} \qquad \begin{cases} Q^\dagger |k; l\rangle_+ = 0, \\ Q^\dagger |k; l\rangle_- = \sqrt{2(k-l)} |k; l\rangle_+. \end{cases} \qquad (57)$$

It is also useful to define the operator Q_1 as in Eq. (47):

$$Q_1 = Q + Q^\dagger. \qquad (58)$$

It reverses the polarization of a state,

$$Q_1 |k; l\rangle_\epsilon = \sqrt{2(k-l)} |k; l\rangle_{-\epsilon}, \qquad (59)$$

and squares to the energy:

$$Q_1^2 = 2H. \qquad (60)$$

The space of states can be decomposed into subspaces according to the fermion number. In the following, we will concentrate our attention on Q .

$$C^p = \text{Span} \{ |k, a; l, b\rangle_\epsilon \mid F |k, a; l, b\rangle_\epsilon = p |k, a; l, b\rangle_\epsilon \}, \qquad (61a)$$

$$C^{2k} = \text{Span} \{ |k, a; l, b\rangle_+ \}, \qquad (61b)$$

$$C^{2k+1} = \text{Span} \{ |k, a; l, b\rangle_- \}. \qquad (61c)$$

We also define

$$C^+ = \bigoplus_k C^{2k}, \qquad (62a)$$

$$C^- = \bigoplus_k C^{2k+1}, \qquad (62b)$$

$$C^* = C^+ \oplus C^- = \bigoplus_p C^p. \qquad (62c)$$

One verifies easily that

$$Q : C^p \rightarrow C^{p+1} \qquad (63)$$

(and conversely $Q^\dagger : C^p \rightarrow C^{p-1}$). We can now construct the co-chain complex

$$0 \hookrightarrow C^0 \xrightarrow{Q} C^1 \xrightarrow{Q} \dots \xrightarrow{Q} C^N \xrightarrow{Q} 0. \quad (64)$$

Let us now study the cohomology of such a complex. The 0-energy states $|k, a; k, b\rangle_\epsilon$ and the negative polarization states $|k, a; l, b\rangle_-$ are Q -closed. On the other hand, negative polarization states (with $k \neq l$) are also Q -exact, such that the cohomology coincides with the set of supersymmetric ground states:

$$\bigoplus_p H^p(Q) = \text{Span} \{ |k, a; l, b\rangle_\epsilon \mid H|k, a; l, b\rangle_\epsilon = 0 \} = \text{Span} \{ |k, a; k, b\rangle_\epsilon \}. \quad (65)$$

Moreover, all the states with $a \neq b$ are paired (opposite parities). This means that when taking the Euler number, only the $|k, a; k, a\rangle$ states (perfect matchings) contribute:

$$\chi = \text{Tr} (-1)^F = \sum_p (-1)^p \dim [H^p(Q)] = \sum_p N_p. \quad (66)$$

As we remarked above, diagrammatically, ground states are configurations with vanishing total winding number. The ones contributing to the Euler number are only those that do not contain any loops.

A different invariant can be constructed by taking the trace of the $(-1)^F z^K$ operator (which is still a conserved quantity since it is a function of conserved operators). It is easy to see that it is given by

$$\chi(z) = \text{Tr} \left[(-1)^F z^K \right] = \sum_{k, \epsilon} (-1)^p z^k \dim [H^p(Q)] = \sum_k z^k N_k, \quad (67)$$

where $p = 2k - \frac{1}{2}(\epsilon - 1)$. This is the Poincaré polynomial for the sequence in Eq. (64) and in particular, $\chi(1) = \chi$. Moreover, $\chi(-z)$ is by construction the partition function for the free Majorana fermion on the lattice.

It is worth stressing that even if, as it is often the case, the zero-modes alone are enough to describe important features of the physics of the system such as the partition function, we have complete control over all the states in the theory. In Appendix B, the generating functions capturing all loop states are given.

4.2 Example: One square on the cylinder

To illustrate the above, we now present the smallest possible example on the cylinder, consisting only of one square. The five possible matchings and their quantum numbers are shown in Figure 9. They combine into 25 loop configurations, which are, sorted into their co-chain groups according to total winding number, depicted in Table 1.

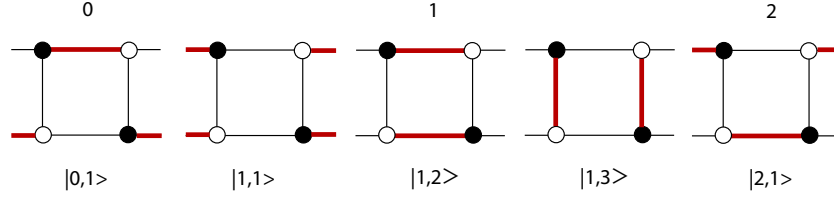


Figure 9: Matchings for the square on the cylinder

The partition function can easily be found by inspection and reads:

$$P(z) = z \left(-\frac{1}{z} + 3 - z \right). \quad (68)$$

The generating function for this example reads

$$G(\mathbf{q}, \mathbf{z}, y) = 1 + 3y^2z + y^4z^2 + (1 + y) \left[3y^2z + 3q \left(y^2z + y^4z^2 \right) + q^2y^4z^2 \right]. \quad (69)$$

4.3 Loops as operators

In this section, we introduce a different notation for the loops that will allow us to make contact with the geometric and gauge theory descriptions in Sec. 5 and 6. Each perfect matching can be seen as a pure state in a quantum system obeying a normalization condition $\langle k, a | l, b \rangle = \delta_{kl} \delta_{ab}$. The general (quantum) configuration for the system is obtained as a linear combination

$$|\Psi\rangle = \sum_k \sum_a \lambda_{k,a} |k, a\rangle, \quad (70)$$

where $\lambda_{k,a}$ are complex parameters normalized as usual $\sum_{k,a} |\lambda_{k,a}|^2 = 1$.

Using this point of view, a loop can be identified with a map going from a state $|k, a\rangle$ to a state $|l, b\rangle$ and as such is represented in bracket notation by $|l, b\rangle\langle k, a|$ acting as

$$(|l, b\rangle\langle k, a|) |k', a'\rangle = \delta_{kk'} \delta_{aa'} |l, b\rangle. \quad (71)$$

The linear combination of two loops is still well defined, but a new operation is naturally defined by the product of two loops:

$$(|l, b\rangle\langle k, a|) \times (|l', b'\rangle\langle k', a'|) \mapsto |l, b\rangle\langle k', a'| \delta_{kl'} \delta_{ab'}. \quad (72)$$

Note that this is the usual path algebra on a complete graph whose nodes are labelled by $|k, a\rangle$. It is useful to introduce a new representation for our states. Consider a graph with N nodes arranged on the lattice \mathbb{N}^2 at coordinates (k, a) , and represent the loop $|l, b\rangle\langle k, a|$ as

$k-l$	C^0	C^1	C^2	C^3	C^4	C^5
2	-	-	-	-	$ 2, 1; 0, 1\rangle_+$ 	$ 2, 1; 0, 1\rangle_-$
1	-	-	$ 1, 3; 0, 1\rangle_+$ 	$ 1, 3; 0, 1\rangle_-$ 	$ 2, 1; 1, 3\rangle_+$ 	$ 2, 1; 1, 3\rangle_-$
1	-	-	$ 1, 2; 0, 1\rangle_+$ 	$ 1, 2; 0, 1\rangle_-$ 	$ 2, 1; 1, 2\rangle_+$ 	$ 2, 1; 1, 2\rangle_-$
1	-	-	$ 1, 1; 0, 1\rangle_+$ 	$ 1, 1; 0, 1\rangle_-$ 	$ 2, 1; 1, 1\rangle_+$ 	$ 2, 1; 1, 1\rangle_-$
0	-	-	$ 1, 3; 1, 2\rangle_+$ 	$ 1, 3; 1, 2\rangle_-$ 	-	-
0	-	-	$ 1, 3; 1, 1\rangle_+$ 	$ 1, 3; 1, 1\rangle_-$ 	-	-
0	-	-	$ 1, 2; 1, 1\rangle_+$ 	$ 1, 2; 1, 1\rangle_-$ 	-	-
0	-	-	$ 1, 3; 1, 3\rangle$ 	-	-	-
0	-	-	$ 1, 2; 1, 2\rangle$ 	-	-	-
0	$ 0, 1; 0, 1\rangle$ 	-	$ 1, 1; 1, 1\rangle$ 	-	$ 2, 1; 2, 1\rangle$ 	-

Table 1: Co-chain groups for the square on the cylinder

the arrow from (k, a) to (l, b) . Our system of loops corresponds to a complete graph with double lines pointing in opposite directions plus a loop on top of each vertex (this is a state graph, see Fig. 10(a)). The co-chain groups (Abelian, freely generated by the loops) receive the following interpretation:

- C^{2p} is the group generated by the loops mapping from a state with winding p to a state with winding smaller than p (arrows pointing left), from a state with winding p to another one with a smaller degeneracy number (arrows pointing down), or from a state to itself (loops). Fig. 10(b);
- C^{2p+1} is the group generated by the loops mapping from a state with winding smaller than p to one with winding p (arrows pointing right), or from a state with winding p to another with the same winding and higher degeneracy number (arrows pointing up). Fig. 10(c).

In terms of the state graph, this means that the differential map $Q_{2p} : C^{2p} \rightarrow C^{2p+1}$ maps every arrow with a non-vanishing left component to its opposite and annihilates all the others:

$$Q_{2p} : |l, b\rangle\langle p, a| \mapsto |p, a\rangle\langle l, b|, \quad (73)$$

$$Q_{2p} : |p, b\rangle\langle p, a| \mapsto 0. \quad (74)$$

On the other hand, $Q_{2p+1} : C^{2p+1} \rightarrow C^{2p+2}$ annihilates every map

$$Q_{2p+1} : |p, a\rangle\langle l, b| \mapsto 0. \quad (75)$$

It is immediate to see that when considering the cohomology one finds:

- $H^{2p} \subset C^{2p}$ is generated by downwards pointing arrows and loops. Fig. 10(d);
- $H^{2p+1} \subset C^{2p+1}$ is generated by upwards pointing arrows. Fig. 10(e).

This implies in turn that taking the Euler character, only the loops survive since upward and downward pointing arrows are paired and counted with opposite signs (Fig. 10(f)). They are in one-to-one correspondence with the nodes and all counted with (+) sign, such that

$$\chi = \sum_p (-1)^p \dim(H^p) = \sum_p N_p = N. \quad (76)$$

4.4 The dimer model on the torus and supersymmetric QM

We are now ready to pass to the actual case of interest, *i.e.* to extend the categorification construction of Sec. 4.1 to graphs embedded on a torus. Now we have two non-trivial cycles, so each matching has two weights, k_z and k_w , as explained in Sec. 2. These weights will be treated on a different footing, but the final result will restore the expected symmetry.

The notation is modified as follows:

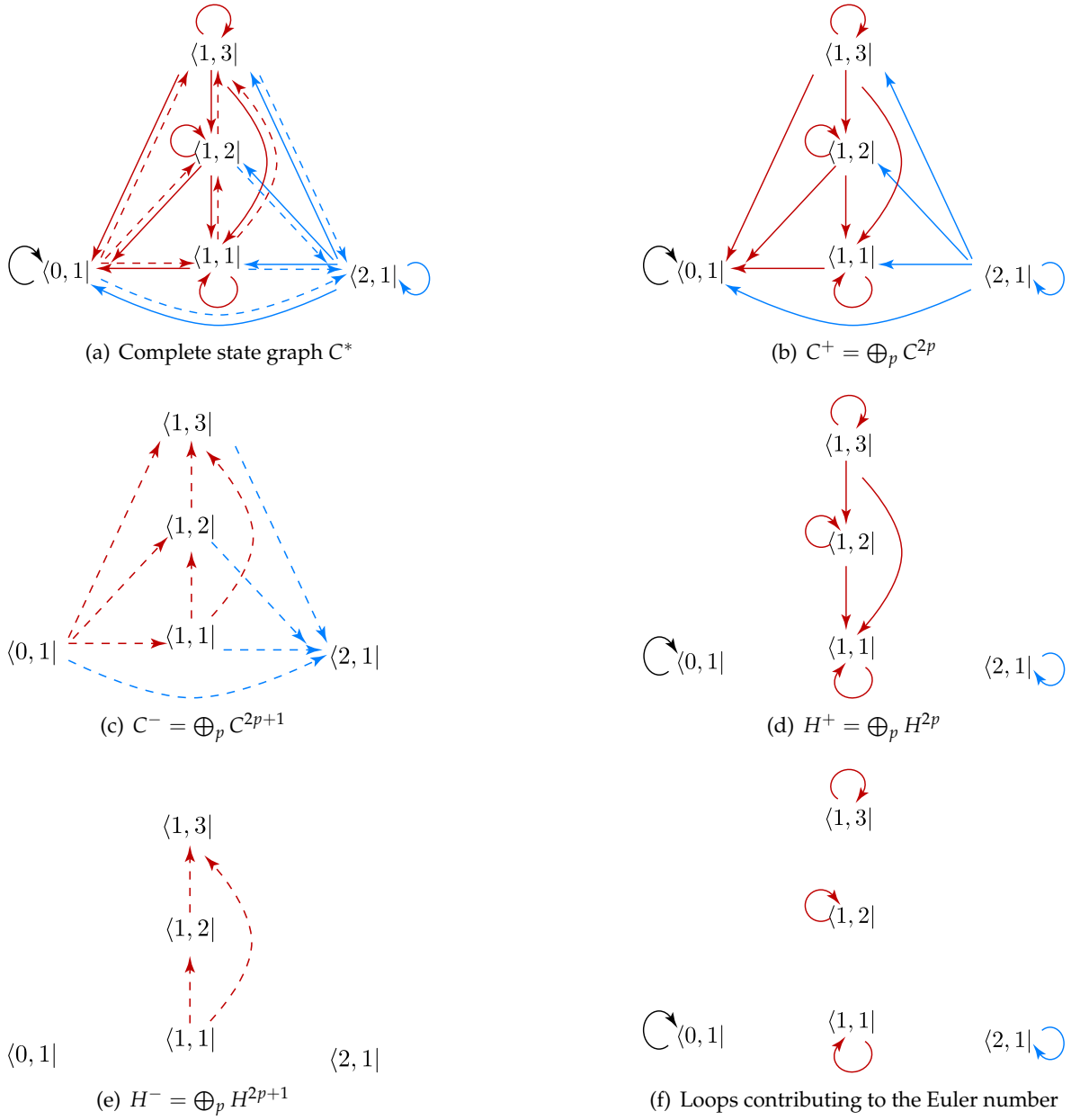


Figure 10: State graph for the dimer model in Sec. 4.2

- a perfect matching is labelled as $|\mathbf{k}, a\rangle\rangle$, where \mathbf{k} is the vector $\mathbf{k} = (k_z, k_w)$ and $a = 1, \dots, N_{\mathbf{k}}$;
- a loop is the combination of two matchings and is labelled by $|\mathbf{k}, a; \mathbf{l}, b\rangle_{\epsilon}$, where $k_z \geq l_z$, $\epsilon = \pm 1$.

$$\begin{aligned}
|\mathbf{k}, a; \mathbf{l}, b\rangle_+ &= |\mathbf{k}, a\rangle\rangle \otimes |\mathbf{l}, b\rangle\rangle && \text{if } \mathbf{k} \succ \mathbf{l}, \\
|\mathbf{k}, a; \mathbf{l}, b\rangle_- &= |\mathbf{l}, b\rangle\rangle \otimes |\mathbf{k}, a\rangle\rangle && \text{if } \mathbf{k} \succ \mathbf{l}, \\
|\mathbf{k}, a; \mathbf{k}, b\rangle_+ &= |\mathbf{k}, a\rangle\rangle \otimes |\mathbf{k}, b\rangle\rangle && \text{if } a > b, \\
|\mathbf{k}, a; \mathbf{k}, b\rangle_- &= |\mathbf{k}, b\rangle\rangle \otimes |\mathbf{k}, a\rangle\rangle && \text{if } a > b, \\
|\mathbf{k}, a; \mathbf{k}, a\rangle_+ &= |\mathbf{k}, a\rangle\rangle \otimes |\mathbf{k}, a\rangle\rangle, \\
|\mathbf{k}, a; \mathbf{k}, a\rangle_- &= 0,
\end{aligned} \tag{77}$$

where $\mathbf{k} \succ \mathbf{l}$ if $k_z > l_z$ or if $\{k_z = l_z, k_w > l_w\}$. This corresponds to lexicographic order.

Again, the loops can be seen as eigenstates for the following operators:

$$H |\mathbf{k}; \mathbf{l}\rangle_{\epsilon} = (k_z - l_z) |\mathbf{k}; \mathbf{l}\rangle_{\epsilon}, \tag{78}$$

$$K_z |\mathbf{k}; \mathbf{l}\rangle_{\epsilon} = k_z |\mathbf{k}; \mathbf{l}\rangle_{\epsilon}, \tag{79}$$

$$K_w |\mathbf{k}; \mathbf{l}\rangle_{\epsilon} = \max(k_w, l_w) |\mathbf{k}; \mathbf{l}\rangle_{\epsilon}, \tag{80}$$

$$\Pi |\mathbf{k}; \mathbf{l}\rangle_{\epsilon} = \epsilon |\mathbf{k}; \mathbf{l}\rangle_{\epsilon}. \tag{81}$$

As opposed to the example on the cylinder, a loop state now comes with two natural signs, $\epsilon_z = \text{sign}(k_z - l_z)$, and $\epsilon_w = \text{sign}(k_w - l_w)$. For the grading by the fermion number, we assign only one sign ϵ to each loop state according to Table 2. This is achieved by

ϵ_z	ϵ_w	ϵ
+	+	+
-	-	-
+	-	+
-	+	-

Table 2: Sign table for torus loop states

$$\epsilon = \epsilon_z + (1 - \epsilon_z^2) \epsilon_w. \tag{82}$$

By choosing the right order on the perfect matchings of the same weight and choosing a sign for some loop configurations of winding number 0, the signs of the overall winding numbers around the z and w cycles can be brought to correspondence with the signs ϵ_z, ϵ_w defined above. We assign a sign to an oriented loop by choosing a right handed (counterclockwise) system to have positive sign and a left handed (clockwise) to have negative sign. The signs of a loop configuration are determined by the overall winding number around the cycles.

Only in cases with an equal number of loops winding a cycle in opposite directions, a sign has to be chosen arbitrarily.

The fermion number operator only depends on K_z and is defined by

$$F = 2 K_z - \frac{1}{2} (\Pi - 1) . \quad (83)$$

States can be again collected into subspaces according to the eigenvalues of F , but in this case, we have an extra grading given by k_w . Since $[F, K_w] = 0$, we obtain a direct sum structure, and define:

$$C^p = \bigoplus_{q=0}^M C^{p,q} , \quad (84)$$

$$C^{p,q} = \text{Span} \{ | \mathbf{k}; \mathbf{l} \rangle_\epsilon \mid F | \mathbf{k}; \mathbf{l} \rangle_\epsilon = p, K_w | \mathbf{k}; \mathbf{l} \rangle_\epsilon = q \} . \quad (85)$$

The differential operators (or supercharges) are defined precisely as in Eq. (57)

$$\begin{cases} Q | \mathbf{k}; \mathbf{l} \rangle_+ = \sqrt{2(k_z - l_z)} | \mathbf{k}; \mathbf{l} \rangle_- , \\ Q | \mathbf{k}; \mathbf{l} \rangle_- = 0. \end{cases} \quad \begin{cases} Q^\dagger | \mathbf{k}; \mathbf{l} \rangle_+ = 0, \\ Q^\dagger | \mathbf{k}; \mathbf{l} \rangle_- = \sqrt{2(k_z - l_z)} | \mathbf{k}; \mathbf{l} \rangle_+ , \end{cases} \quad (86)$$

and it is immediate to verify that they respect the grading since $[K_w, Q] = [K_w, Q^\dagger] = 0$. Again we concentrate on Q . It can be decomposed into the sum

$$Q_p = \sum_{q=0}^M Q_{p,q} , \quad (87)$$

where

$$Q_p : C^{p,q} \rightarrow C^{p+1,q} , \quad q = 0, \dots, M. \quad (88)$$

As a result, the C^* complex is decomposed into $C_{*,q}$ complexes:

$$\begin{array}{ccccccccc} 0 & \hookrightarrow & C^{0,M} & \xrightarrow{Q_{0,M}} & C^{1,M} & \xrightarrow{Q_{1,M}} & \dots & \xrightarrow{Q_{N-1,M}} & C^{N,M} & \xrightarrow{Q_{N,M}} & 0, \\ & & & & & & \dots & & & & \\ 0 & \hookrightarrow & C^{0,q} & \xrightarrow{Q_{0,q}} & C^{1,q} & \xrightarrow{Q_{1,q}} & \dots & \xrightarrow{Q_{N-1,q}} & C^{N,q} & \xrightarrow{Q_{N,q}} & 0, \\ & & & & & & \dots & & & & \\ 0 & \hookrightarrow & C^{0,0} & \xrightarrow{Q_{0,0}} & C^{1,0} & \xrightarrow{Q_{1,0}} & \dots & \xrightarrow{Q_{N-1,0}} & C^{N,0} & \xrightarrow{Q_{N,0}} & 0. \end{array} \quad (89)$$

The analysis of the cohomology is the same as in the case of the cylinder and one can

easily convince oneself that it consists of states of zero energy:

$$\bigoplus_{p,q} H^{p,q} = \text{Span} \{ | \mathbf{k}, a; \mathbf{l}, b \rangle_\epsilon \mid k_z = l_z \}. \quad (90)$$

Once more, only the states that are in one-to-one correspondence with the perfect matchings (*i.e.* the ones that do not contain non-trivial closed loops) are not paired and thus survive the projection by the $(-1)^F$ operator:

$$\chi(w) = \text{Tr} \left[(-1)^F w^{K_w} \right] = \sum_{p,q} w^q N_{p,q}, \quad (91)$$

where we introduced the variable w to keep track of the internal grading. The partition function described in Eq. (8) is obtained as the trace of the operator $(-1)^{F+K_z K_w} (-z)^{K_z} (-w)^{K_w}$:

$$P(z, w) = \text{Tr} \left[(-1)^{F+K_z K_w} (-z)^{K_z} (-w)^{K_w} \right] = \sum_{p,q} (-1)^{p+q+pq} z^p w^q N_{p,q}. \quad (92)$$

Note the presence of the factor $(-1)^{p+q+pq}$, which coincides with the signature of the spin structure. Because of this, the expression differs from the Poincaré polynomial for the graded complex

$$\chi(z, w) = \sum_{p,q} z^p w^q N_{p,q}. \quad (93)$$

The two polynomials, on the other hand, contain the same information and one can pass from one to the other using the identity

$$2\chi(z, w) = -P(z, w) + P(-z, w) + P(z, -w) + P(-z, -w). \quad (94)$$

In particular, $\chi(w) = \chi(-1, w)$ and $\chi(1, 1)$ is the overall number of perfect matchings on the graph. As already remarked at the beginning of this section, it is worth emphasizing that the choice of the cycles is arbitrary. This means in particular that one could have used K_w to construct the Fermion number operator and K_z as an internal grading without affecting the final result.

The generalization to graphs embedded on higher-genus Riemann surfaces is straightforward and leads to a $(2g - 1)$ -graded complex.

A simple example to illustrate the above is given in Appendix C.

5 Gauge theory interpretation: Preliminaries

As mentioned in the introduction, there exists a correspondence between quiver gauge theories describing D -branes probing singular toric surfaces and the dimer model [14, 15]. We will make use of it to re-interpret the loops in terms of the quiver gauge theory and the toric

geometry. We will quickly summarize the necessary knowledge of quiver gauge theories and this correspondence in the following.

5.1 The quiver gauge theory

Consider $D3$ -branes in type IIB string theory probing a Calabi–Yau X . They correspond to BPS B -type branes given by points on X . If the D -branes are placed at a singularity, they are expected to decay into a collection of so-called *fractional* branes. The resulting world-volume gauge theory can be summarized in a *quiver* graph Q_X as follows. Each constituent brane appearing with multiplicity N_i corresponds to a $U(N_i)$ gauge group which is represented as a node in the quiver graph. The massless open strings stretching between the fractional branes correspond to chiral fields in the (\overline{N}_i, N_j) representation and are depicted as arrows pointing from the $U(N_i)$ -node to the $U(N_j)$ -node in the diagram. For the theory to be anomaly free, the number of arrows a_{ik} going from node N_i to node N_k (in our convention $a_{ki} = -a_{ik}$) must fulfill

$$\sum_i N_i a_{ik} = 0, \quad \forall k. \quad (95)$$

If the ranks of all gauge groups are equal, this reduces to the number of incoming and outgoing arrows being equal at each node.

We will be concentrating on the case of the Calabi–Yau X being the cone over a singular toric surface S .

To fully capture the physics of the D -branes, they must be described in terms of the (bounded) derived category of coherent sheaves $D^b(X)$. A full explanation of the machinery of the derived category is beyond the scope of this paper, the reader is therefore referred to [48]. Luckily, we can avoid working directly in $D^b(X)$ by using so-called *exceptional collections* of sheaves supported on a partial resolution of the singular surface S . In our case, these sheaves can be mostly thought of as line bundles. The exceptional collections form a convenient basis for the fractional branes and it is possible to construct the quiver from a given exceptional collection and vice versa [49]. The whole treatment is based on the fact that the derived category of coherent sheaves is equivalent to the derived category of quiver representations.

The open strings in the topological sector between two B -branes A and B are parametrized by $\oplus_p \text{Ext}^p(A, B)$. The mass of such an open string between two branes with the same grade is given in string units by

$$m^2 = \frac{1}{2}(p - 1). \quad (96)$$

From this, we learn that the massless open strings (*i.e.* the arrows in the quiver) are counted by Ext^1 , while Ext^0 counts the tachyons. For $p > 1$, the strings are very massive and are not seen by the quiver gauge theory.

If oriented loops appear in a quiver (which is always the case for our quiver gauge theories because of the anomaly–freedom condition in Eq. (95)), the quiver representations become infinite dimensional, causing the methods employed in [49] to fail. Fortunately, this problem can be evaded by considering acyclic subquivers. Some of the arrows of the gauge theory quiver Q_X are linked to the properties of the surface S itself, while the others parametrize the embedding of S in the Calabi–Yau X . Deleting these latter arrows removes all oriented loops. The resulting quiver, Q_S , allows an ordering relation and is also called the Beilinson or Bondal quiver in the literature.

The derived category of coherent sheaves on S , $D^b(S)$, is equivalent to the derived category of quiver representations for Q_S , denoted by $D^b(A - \text{mod})$ (where A is the path algebra of Q_S). The basic representations L_i of the path algebra A are associated to the fractional branes at the nodes of the quiver. The arrows in the quiver are thus associated with the $\text{Ext}^1(L_i, L_j)$. The $\text{Ext}^2(L_i, L_j)$ correspond to relations in the quiver which the paths must obey. There is another quiver representation given by the projective objects P_i , which are the subspaces of A generated by all paths starting at node i . The sheaves in the exceptional collections we consider are the projective objects P_i , which are in some sense dual to the fractional branes L_i .

Let us illuminate a bit the connection between the quivers Q_S and Q_X and its geometrical meaning. Consider the embedding of the surface S into X via $i : S \hookrightarrow X$. A D -brane in S can obviously also be regarded as a D -brane in X , *i.e.* we can map objects in $D^b(S)$ injectively to objects in $D^b(X)$ using i_* . Since there might be more morphisms in $D^b(X)$ than $D^b(S)$, some of the open strings between two branes in S may live in X but outside of S . This fact is captured by the relation

$$\text{Ext}_X^1(i_*L_i, i_*L_j) = \text{Ext}_S^1(L_i, L_j) \oplus \text{Ext}_S^2(L_j, L_i). \quad (97)$$

Thus, the decomposition of the arrows of the full quiver Q_X into Ext^1 and Ext^2 on S accounts for the embedding of S in X .

5.2 Exceptional collections and helices

In this section, we collect the definitions on exceptional collections necessary for later chapters. An (ordered) collection of sheaves $\{\mathcal{F}_0, \dots, \mathcal{F}_{n-1}\}$ on S is called *exceptional* if

$$\text{Ext}_S^0(\mathcal{F}_i, \mathcal{F}_i) = \mathbb{C} \quad (98a)$$

$$\text{Ext}_S^p(\mathcal{F}_i, \mathcal{F}_i) = 0, \quad p \geq 1 \quad (98b)$$

$$\text{Ext}_S^p(\mathcal{F}_i, \mathcal{F}_j) = 0, \quad i > j. \quad (98c)$$

The collection is called *strongly exceptional*, if $\text{Ext}_S^p(\mathcal{F}_i, \mathcal{F}_j) = 0$ for $p \neq 0$ and *complete* if it generates $D^b(S)$. Since the D -branes on S can wrap 0-, 2- and 4-cycles, a collection must contain n sheaves to be complete, where $n = \text{sum over all Betti numbers} (= \chi(S))$. For physics, the collection being strong means that the basis of fractional branes it generates does not contain ghost matter.

Exceptional collections can be transformed into new exceptional collections by left and right *mutations*, which represent an action of the braid group on the set of possible collections. On a neighboring pair of sheaves in an exceptional collection, the mutations act as

$$L_i : (E_i, E_{i+1}) \mapsto (L_{E_i} E_{i+1}, E_i), \quad (99)$$

$$R_i : (E_i, E_{i+1}) \mapsto (E_{i+1}, R_{E_{i+1}} E_i). \quad (100)$$

The sheaves $L_{E_i} E_{i+1}$ and $R_{E_{i+1}} E_i$ are defined via short exact sequences, see [50, 51]. Left and right mutations can be seen as braiding and unbraiding. A *helix* \mathcal{H} is an infinite collection of coherent sheaves $\{\mathcal{F}_i\}_{i \in \mathbb{Z}}$ such that

- (a) for any $i \in \mathbb{Z}$, $\{\mathcal{F}_{i+1}, \dots, \mathcal{F}_{i+n}\}$ is an exceptional collection.
- (b) $R^{n-1} \mathcal{F}_i = \mathcal{F}_{i+n}$.

The name stems from the fact that after moving n steps to the right, one is back at the original place up to a translation. n is called the *period* n of \mathcal{H} . Each collection of the form $\{\mathcal{F}_{i+1}, \dots, \mathcal{F}_{i+n}\}$ is called a *foundation* of the helix and \mathcal{H} is uniquely determined by each of its foundations.

5.3 The correspondence

Here we quickly summarize the correspondence worked out in [14, 15].

1. Start with a toric quiver gauge theory, given by a quiver graph and its tree-level superpotential.
2. Draw the quiver diagram on a torus, such that each of the terms of the superpotential corresponds to a plaquette. The resulting graph is called the *periodic quiver*.
3. Take the graph dual of this graph (i.e. vertices become faces, faces become vertices and edges remain edges). Colour the vertices coming from the faces associated to a superpotential term with negative sign black; the ones coming from a positive term colour white. The resulting graph is bipartite and also lives on a torus.
4. Solve the dimer model on this graph by taking the Pfaffian of the Kasteleyn matrix. This yields the Newton polynomial. The associated *Newton polygon* is given by taking

the exponents of the monomials in zw to be coordinates in the (z, w) -plane. The resulting polygon is exactly the toric diagram of the surface the quiver gauge theory comes from!

The singular surface S is specified by the corners of the toric diagram. These corner vertices each correspond to Weil divisors and therefore to line bundles. The fully resolved surface is given by adding all the points lying in the intersection of the convex hull of the polygon and the integer \mathbb{Z}^2 -lattice to the toric diagram. Each such vertex corresponds to an exceptional divisor which is blown up to resolve the singularity. The surface S can also be resolved partially by blowing up only part of the exceptional divisors. Passing from one partial resolution S' corresponding to the exceptional divisor E' being blown up to another partial resolution S'' with E'' being blown up corresponds to a sequence of birational transformations (blow down E' and blow up E'' instead).

The vertices of the toric diagram can be labeled with the multiplicities of the perfect matchings with the corresponding weight. There are certain patterns in the multiplicities which are worth pointing out:

- The vertices at the corners of the toric diagram always have multiplicity one, since they correspond to the highest or lowest weight states in either z or w , which are unique.
- The multiplicities on the edges of the graph follow the rule of Pascal's triangle (i.e. 1, 2, 1 or 1, 3, 3, 1, etc.). Indeed, the polynomial consisting only of the monomials associated to the vertices of an edge has the form $(z + w)^n$, or can be brought to this form by multiplication with a prefactor $z^{n_0}w^{m_0}$ or by redefinition of the variables.

For the multiplicities of the vertices in the interior of the toric diagram, a pattern is much less obvious.

We illustrate the above by the example of one square on the torus, which corresponds to the quiver gauge theory on \mathbb{F}_0 in Figure 11.

The tree-level superpotential is given by

$$W = -2 X_{DC}X_{CA}X_{AB}X_{BD} + 2 X_{CA}X_{AB}X_{BD}X_{DC}, \quad (101)$$

the Newton polynomial is

$$P(z, w) = zw \left(-\frac{1}{z} - \frac{1}{w} + 4 - z - w \right). \quad (102)$$

6 Gauge theory interpretation: Results

In Section 4.3, we have seen that our fermion loop configurations can be interpreted as maps from one perfect matching to another. Geometrically, a marked difference exists between the

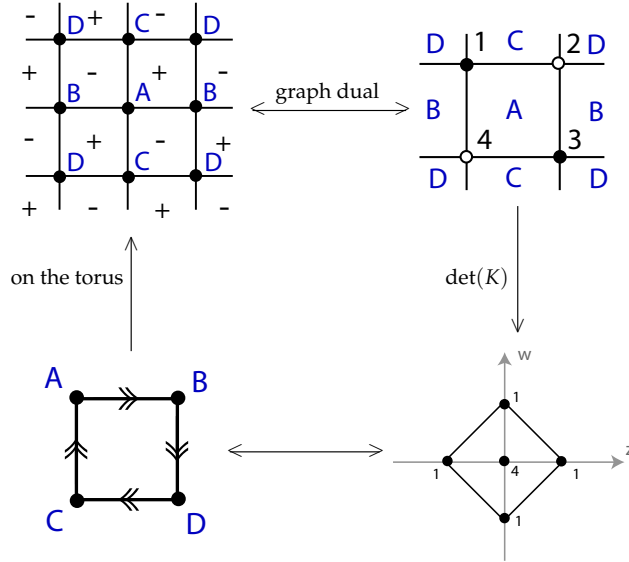


Figure 11: Web of correspondences for one square on the torus/ quiver gauge theory on \mathbb{F}_0

inner vertices of a toric diagram and those on the boundary. The inner vertices correspond to exceptional divisors and are compact. The vertices on the boundary must be subdivided into the ones at the corners of the diagram and the others. The latter are also exceptional divisors and are of the form $\mathbb{P}^1 \times \mathbb{C}$ with possible blow-ups, *i.e.* have a compact and a non-compact factor. The corner vertices are non-compact and have the form $\mathbb{C} \times \mathbb{C}$ plus possible blow-ups. It is therefore not surprising that it makes a difference whether we only map between internal matchings or if boundary matchings appear on one side of the map. When the size of the graph is very large, *i.e.* $N, M \rightarrow \infty$, maps between internal matchings indeed are the generic case.

It was shown in [17] that for each internal matching $\text{PM}_i \in \{\text{PM}^{\text{int}}\}$, an acyclic quiver Q_{PM_i} is obtained by deleting all edges which are part of PM_i from the dual quiver Q_X . We can construct an exceptional collection of sheaves for each such Q_{PM_i} . We associate Q_{PM_i} to the quiver Q_{S_i} corresponding to the partial resolution S_i of S obtained by blowing up the divisor E_i to which PM_i belongs. The acyclic quiver Q_{S_i} represents the system as seen by an observer living only on S , while from the point of view of the whole Calabi–Yau X , the low-energy theory remains unchanged, regardless of the resolution. The different Q_{S_i} associated to perfect matchings belonging to the same internal point can be seen as different ways the gauge theory is embedded in the surface $S_i \subset X$. The acyclic quivers associated to different resolutions S_i and S_j also correspond to different decompositions of the arrows in Q_X into Ext_S^1 and Ext_S^2 , see Eq. (97), but this difference should rather be seen as due to the different topologies of the partially resolved surfaces S_i, S_j the exceptional collections are supported on.

On the quiver side, a map between internal matchings corresponds thus to a map $f_{ji} : Q_{S_i} \mapsto Q_{S_j}$, while on the geometry side, it corresponds to mapping from one exceptional collection to another. These maps are *always graph isomorphisms of the full quiver* Q_X , in the sense that the adjacency remains unchanged and only the labels of the nodes are permuted. This means that the physical gauge quiver Q_X remains unchanged by the loop maps, *i.e.* the quiver gauge theory is too coarse to see their effect. At the level of the acyclic quivers Q_{S_i} , the maps correspond to gauge dualities. Geometrically, the decomposition of the arrows of Q_X into Ext_S^1 and Ext_S^2 changes, which corresponds to a change of embedding.

In the case of a boundary perfect matching, cycles will remain in the reduced quiver $Q_{\text{PM}_{bd}}$ which causes the quiver representation to be infinite dimensional and the construction of the exceptional collection to fail. This failure of the known methods to extract useful information for these cases prevents us from giving a satisfactory interpretation of maps involving boundary matchings.

There is one special case in which the loop states admit a direct interpretation in the quiver gauge theory. It is the case of loops arising from the composition of two adjacent boundary matchings. It was noticed in [16] that this results in a so-called *zig-zag path*. A zig-zag path is a path which turns alternately maximally left and maximally right at the vertices. This maximal turning condition results in also the edges in the dual graph forming a closed path, which is not the case for a general path. A closed zig-zag path on the dimer model graph \mathcal{G} therefore results in a closed zig-zag path in the dual quiver, which corresponds to a gauge invariant trace operator.

6.1 Matchings and acyclic quivers

The problem of finding a minimal set of arcs in a directed graph upon the deletion of which the graph becomes acyclic is well studied in mathematics and computer science [52]. Such a set is called a minimal *feedback arc set* (FAS). There exists a precise relation between the problem of finding all FAS of a digraph and the problem of identifying all the perfect matchings in its dual graph.

Consider a bipartite plane graph \mathcal{G} with N nodes and its graph dual \mathcal{G}' . The one-cycles in \mathcal{G}' are generated by the plaquettes $\{p_j\}_{j=1}^N$ which correspond to the vertices of \mathcal{G} . Removing the edge e_{ij} shared by the cycles p_i and p_j breaks both cycles. A minimal FAS is obtained as the collection of $N/2$ edges $\{e_{i_k j_k}\}_{k=1}^{N/2}$ shared by disjoint pairs of plaquettes p_{i_k} and p_{j_k} . In the dual graph \mathcal{G} , this corresponds to selecting a set of edges joining all the nodes and touching all of them only once. In other words, the FAS in \mathcal{G}' is a perfect matching in \mathcal{G} . The situation is different when \mathcal{G} is embedded on a Riemann surface of genus $g > 0$, because in addition to the one-cycles generated by the plaquettes, there are $2g$ equivalence classes of cycles of non-trivial holonomy. In this case, the winding cycles in \mathcal{G}' are generated by the zig-zag paths. It follows that being a perfect matching in \mathcal{G} is only a necessary condition for

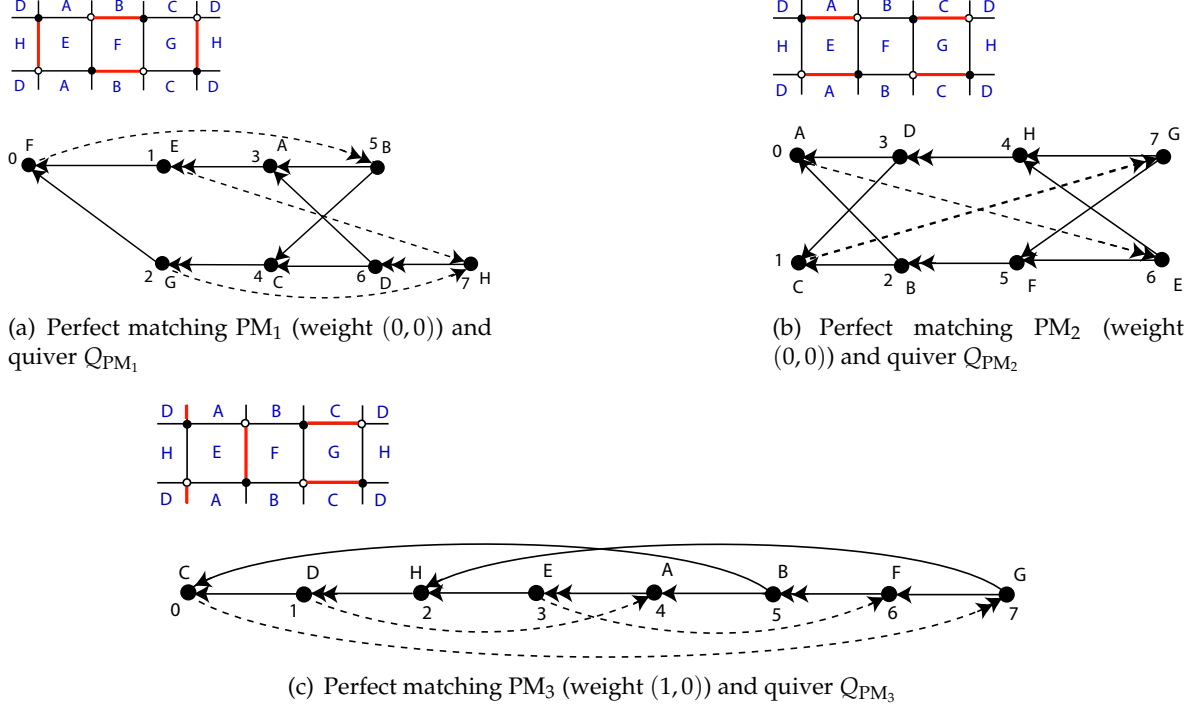


Figure 12: Example: Three inner perfect matchings and associated acyclic quivers

a set of edges to be a FAS in \mathcal{G} . It was shown in [17] that a perfect matching corresponding to an internal point in the toric diagram is always a FAS. Removing a boundary matching, on the other hand, always preserves at least one zig-zag path.

As mentioned before, the gauge quiver Q_X is the graph dual of the graph \mathcal{G} on which the dimer model lives. The acyclic quiver Q_{S_n} is obtained from Q_X by deleting all the edges contained in the n th perfect matching $PM_n \in \{PM^{int}\}$. The deleted arrows are represented by dashed lines and correspond to relations in the quiver, *i.e.* Ext^2 s. Such an acyclic quiver allows an ordering of its nodes such that there are no arrows between the nodes i and j if $i < j$. If Q_S has more than one starting or end point, an ordering ambiguity arises. Indeed, Q_S is in general a partially ordered set which requires two ordering relations, say left to right and bottom to top.

The maps $f_{m,n}^{(0,0)}$ corresponding to $(0,0)$ -loops turn out to have a particularly simple structure: *they always correspond to a cyclic permutation of the nodes in one of the two ordering relations (i.e. up to re-ordering in the vertical direction)*. Maps of non-trivial weight correspond to a general permutation of the nodes. In particular, they do not preserve either of the ordering relations. In the following, we will attempt to give these maps an interpretation as gauge dualities of the acyclic quivers Q_{S_i} .

An example of the above maps is given in Figure 12. This example is big enough to have more than one inner point for the toric diagram. Fig. 12.(a) shows a perfect match-

ing of weight $(0,0)$ and the corresponding dual quiver with the deleted edges depicted by dashed arrows. The map from this quiver to the one shown in Fig. 12.(b) obviously corresponds to the cyclic permutation $f_{2,1}^{(0,0)} : (F, E, G, A, C, B, D, H) \mapsto (A, C, B, D, H, F, E, G)$. Graphically, PM_1 can be recovered from PM_2 by first moving G in front of all nodes its arrows are attached to, then E , and finally F . In the process, dashed arrows which change their direction from pointing left to pointing right become solid and solid arrows which change from pointing left to right become dashed. Notice the ordering ambiguity in the vertical direction. We could have ordered Q_{PM_2} also as *e.g.* (C, A, B, D, F, H, E, G) . Now consider the map from Q_{PM_1} to Q_{PM_3} , shown in Fig. 12.(c). It corresponds to the permutation $f_{3,1}^{(1,0)} : (F, E, G, A, C, B, D, H) \mapsto (C, D, H, E, A, B, F, G)$ which has an obviously more complicated structure and does not preserve either ordering relation.

6.2 Seiberg dualities and graph isomorphisms

In the following, we would like to connect the graph isomorphisms of Q_X arising in the maps $f_{m,n}$ to known gauge dualities of the acyclic quivers. Seiberg dualities [53], which are IR dualities between gauge theories, are obvious candidates. It was first remarked in [54] and later elaborated upon in [49, 55] that certain Seiberg dualities are realized as a sequence of exceptional mutations. Here, we are only interested in producing quivers which are subquivers of Q_X . In general, this will not be the case for Seiberg dualities because the rank of the gauge groups can change, as in Eq. (104).

We want to show here that the effect of performing two consecutive Seiberg dualities on the same node is a graph isomorphism on the physical quiver Q_X and a cyclic permutation on the nodes of the quiver Q_S with respect to one of the ordering relations. Let i_0 be a starting node in the quiver, A_{out} the set of endpoints of the arrows starting in i_0 , and A_{in} the set of starting points for the arrows ending in i_0 . The effect of a Seiberg duality on i_0 is the following [56]: i_0 is moved to the left of the nodes in A_{out} , the directions of the arrows coming to and going from i_0 are reversed, and the arrows between A_{out} and A_{in} are changed to preserve consistency. More precisely, for $A \in A_{\text{out}}$ and $B \in A_{\text{in}}$,

$$\begin{cases} a'_{A i_0} = a_{i_0 A}, \\ a'_{i_0 B} = a_{B i_0}, \\ a'_{AB} = a_{AB} - a_{i_0 A} a_{B i_0}, \end{cases} \quad (103)$$

where a_{ij} is the number of arrows going from node i to node j (with the convention $a_{ji} = -a_{ij}$) in the initial quiver Q_S , and a'_{ij} the corresponding in the quiver Q'_S obtained after the duality.

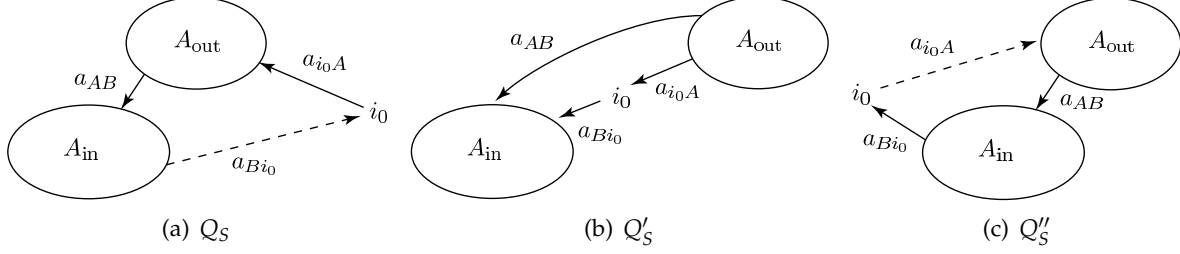


Figure 13: Double Seiberg duality around the node i_0 .

The ranks of the gauge groups are changed as follows:

$$\begin{cases} N'_j = N_j & \text{if } j \neq i_0 \\ N'_{i_0} = \sum_{A \in A_{\text{out}}} a_{i_0 A} N_A - N_{i_0}. \end{cases} \quad (104)$$

In general, $N'_{i_0} \neq N_{i_0}$ and the transformation is not an isomorphism of Q_X . Let us now apply the transformation again on the same node i_0 . The arrows joining i_0 with the other nodes have been reversed, so the role of A_{in} and A_{out} is interchanged:

$$A'_{\text{out}} = A_{\text{in}}, \quad A'_{\text{in}} = A_{\text{out}}. \quad (105)$$

The node i_0 is now moved to the left of $A'_{\text{out}} = A_{\text{in}}$ and the arrows are changed as follows:

$$\begin{cases} a''_{B i_0} = a'_{i_0 B} = a_{B i_0} \\ a''_{i_0 A} = a'_{A i_0} = a_{i_0 A} \\ a''_{BA} = a'_{BA} - a'_{i_0 B} a'_{A i_0} = -(a_{AB} - a_{i_0 A} a_{B i_0}) - a_{i_0 A} a_{B i_0} = a_{BA}. \end{cases} \quad (106)$$

The ranks now read:

$$\begin{cases} N''_j = N'_j = N_j & \text{for } j \neq i_0 \\ N''_{i_0} = \sum_{B \in A'_{\text{out}}} a'_{i_0 B} N'_B - N'_{i_0} = \sum_{B \in A_{\text{in}}} a_{B i_0} N_B - \sum_{A \in A_{\text{out}}} a_{i_0 A} N_A + N_{i_0} = N_{i_0}, \end{cases} \quad (107)$$

where we used the anomaly–cancellation condition around i_0 in Q_X .

As expected, applying the Seiberg duality twice just amounts to an isomorphism of the gauge quiver $Q''_X \sim Q_X$. On the other hand, the node i_0 has been changed from a starting point in Q_S to an end point in $Q_{S''}$, and continuous and dashed arrows from/to i_0 have been interchanged (see Fig. 13).

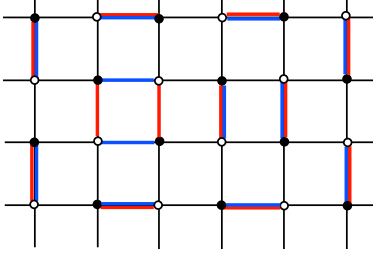


Figure 14: Plaquette move in the square graph

6.3 Interpretation of the $(0, 0)$ -loops

6.3.1 Plaquette moves

With the results of the last section, we can now attempt an interpretation of the $(0, 0)$ -loops, which form the diagonal component of the cohomology $H^{(k,k)}$ for the complex in Eq. (89).

Consider a loop configuration which contains the boundary of a basic plaquette and otherwise only consists of double-line perfect matchings. We define a *plaquette move* to be a map that switches between the two perfect matchings making up the above plaquette loop while leaving the rest of the configuration invariant, see Figure 14. This is obviously a $(0, 0)$ map and corresponds to the minimal loop. It can be shown that the set of loops with windings (\bar{p}, \bar{q}) fixed is connected, with the arcs given by the plaquette moves. It follows that all maps of weight $(0, 0)$ are generated by plaquette moves, *i.e.* we can move between all perfect matchings of fixed weight (\bar{p}, \bar{q}) by a sequence of plaquette moves.

The incoming and outgoing arrows of a node i_0 in Q_X correspond to the edges of the plaquette i_0 in the dual dimer model graph \mathcal{G} . From this dual point of view, the double Seiberg duality described in the last section is precisely a plaquette move since the deleted edges around i_0 are interchanged while all other edges are left untouched [12]. Since any $(0, 0)$ -loop can be decomposed into a product of plaquette moves, it can be interpreted as a sequence of double Seiberg dualities on the acyclic quiver.

It was shown in [57] that a cyclic permutation of the nodes of Q_X corresponds to choosing a different foundation of the same helix. So whenever we map between perfect matchings belonging to the same internal point of the toric diagram, we remain in the same helix.

Moreover, as we already pointed out, a Beilinson quiver $Q_S \subset Q_X$ corresponds to the embedding of a (partially resolved) singular surface S in the Calabi–Yau three-fold X . We can therefore read a $(0, 0)$ -loop as a map between two possible embeddings $i : S \hookrightarrow X$.

6.3.2 Relation to crystal melting and black holes

The dimer configurations of the infinite hexagon graph are in one-to-one correspondence to the configurations of a melting crystal corner [8]. It was shown in [12] that they also corre-

respond to certain BPS black holes given by D -branes wrapping collapsed cycles in $\mathbb{C}^3/\mathbb{Z}_n \times \mathbb{Z}_n$ in the large n limit. The black holes are generated by non-geometry changing flop transitions, which in the dimer picture are identified with so-called *local dimer moves*. The local dimer moves of [12] correspond precisely to the plaquette moves of the hexagon graph. The $S_{\mathbb{R}}^2$ transformations on the fractional branes to which their local dimer moves are related, correspond to the double Seiberg dualities described in Section 6.2. Thus, when specializing to the hexagon graph, the $(0,0)$ -loops are the non-geometry changing flop transitions in $\mathbb{C}^3/\mathbb{Z}_n \times \mathbb{Z}_n$ which generate those BPS black hole charge configurations that are parametrized by the 3d crystal melting configurations. On a plane graph, everything is captured by the $(0,0)$ -loops since no non-trivial winding states exist.

6.4 Interpretation of the loops with non-trivial winding

As mentioned before, the maps corresponding to loops of non-trivial winding result in a general permutation of the nodes of the gauge quiver Q_X . Geometrically, we map from one partial resolution of S to another, which is a birational map. The associated exceptional collections produce equivalent derived categories.

Unlike the $(0,0)$ -maps, loops with non-trivial winding can in general not be written as a sequence of Seiberg dualities. We have seen that plaquette moves cannot generate winding loops, therefore we cannot write the latter as a sequence of double Seiberg dualities. Single Seiberg dualities in general change the ranks of the gauge groups, see Eq. (104), and thus do not lead to a graph isomorphism of the gauge quiver Q_X .

Since the full quiver gauge theory remains unchanged, the action of the weight changing maps $f_{m,n}^{(p,q)}$ on the acyclic quivers can still be seen as a generalized gauge duality on the theory on the (partially resolved) surface S .

What is the geometrical meaning of this? Morally speaking, an exceptional collection forms a basis for the physical branes. All partial resolutions lead to the same quiver gauge theory in X , so at the level of the derived category, the associated exceptional collections are equivalent. Passing from one to the other corresponds to a change of basis. We have seen that with the $(0,0)$ -maps, we change between foundations of a helix. This is a very particular change of basis, which preserves the order of the sheaves in the collection and only amounts to tensoring the canonical bundle a certain number of times to all sheaves in the collection. We have seen on the other hand, that the general permutation of nodes which takes place in a weight-changing map does not preserve the order of the sheaves in the collection. This means that we no longer remain in the same helix. At the level of the sheaves, this map is realized by a general sequence of mutations.

7 Conclusions

In this note, we relate a statistical mechanical system, the dimer model on a torus, to a system of lattice quantum field theory, *i.e.* the massless free fermion. The loop configurations obtained after a diagrammatic expansion of the fermion determinant (Sec. 3.3) can be interpreted as states in SQM after employing categorification techniques inspired by Khovanov's work (Sec. 4). The Newton polynomial of the dimer model becomes the generalized Euler characteristic of a co-chain complex (Sec. 4.4). The states with vanishing overall winding become the supersymmetric ground states of the system. Since all loop states except the double line perfect matchings are paired, taking the Witten index of this system again counts the number of perfect matchings (Eq. (92)).

In the following, we make use of the dimer model–quiver gauge theory correspondence to give the loop configurations an interpretation in yet another picture. Interpreting the loops as maps from one perfect matching to another (Sec. 4.3), maps between internal perfect matchings associated to the same point in the toric diagram become changes of foundation of the associated helix and sequences of double Seiberg dualities in the acyclic quiver (Sec. 6.2). When specializing to the honeycomb graph, the plaquette moves which generate all $(0,0)$ –maps correspond directly to the BPS black hole configurations which are parametrized by crystal melting configurations (Sec. 6.3.2).

Mapping between matchings associated to different internal points is a more severe change and cannot be achieved as a sequence of Seiberg dualities. In the language of exceptional collections, we map from one helix to another.

In Table 3, we summarize the results of this paper by giving a dictionary between the loop states, the fermion states, the gauge theory and the geometry.

From this point, one can go to several different directions for further research.

- The dimer model admits a description as a free fermion model based on a transfer matrix approach (see [29, 30, 31] and also [8]) which, at first sight, is different from the one we introduced in this note. It would be very interesting to clarify the link between these two descriptions.
- Furthermore, it would be interesting to use a more general definition for the Dirac operator on a graph than the one in Eq. (12), to prove the equivalence to the dimer model completely independently of the type of graph and its representation. Indeed, this could provide an elegant solution to the problem of choosing a Dirac operator on a random graph that depends only on the adjacency.
- The algebraic structure we introduce in Sec. 4 also deserves further investigation. A better understanding of the complex and the mapping to SQM might indeed cast a new light on the dual quiver gauge theory.

- A final word must be spent on the geometric interpretation in Sec. 5. To our knowledge, the meaning of the boundary perfect matchings (and, correspondingly, of the infinite-dimensional representations of the path algebras) in terms of derived category is not yet clear. This is an obvious prerequisite to a complete understanding of the geometrical meaning of all the loop states that appear in the theory.

The study of the dimer model, which due to its combinatorial nature provides a relatively easy playground, has proven to be very fruitful thanks to its manifold connections to other physical systems. We believe that these inter-relations have not yet been fully exploited and deserve further attention.

	Loop state	Gauge theory on S	Geometry	Free fermion
$\{\text{PM}^{int}\} \rightarrow \{\text{PM}^{int}\}$	double line PM	Identity	Identity	time evolution with no local charge creation
	$(0,0)$	Seiberg duality	change of foundation in helix	time evolution in which no net charge is created
	$(p,q) \neq (0,0)$	general gauge duality	general sequence of mutation, change of helix, birational transformation	initial conditions with gradient q and creation of net charge p
$\{\text{PM}^{int}\} \leftrightarrow \{\text{PM}^{bd}\}$	no corner PM	?	birational transformation	"
$\{\text{PM}^{bd}\} \rightarrow \{\text{PM}^{bd}\}$	adjacent boundary matchings. Zig-zag path	gauge-invariant multi-trace operator		"
	no corner PM		birational transformation	"

Table 3: Dictionary

Acknowledgements

We would like to thank Luis Álvarez-Gaumé, David Cimasoni, Davide Forcella, Emanuel Scheidegger, and Alberto Zaffaroni for enlightening discussions. Furthermore, we would like to thank David Cimasoni for detailed comments on the manuscript.

D.O. and S.R. would like to thank CERN for hospitality, where part of this work was carried out.

The research of R.D. was supported by a NWO Spinoza grant and the FOM program "String Theory and Quantum Gravity." D.O. is supported in part by INFN and MIUR under contract 2005-024045 and by the European Community's Human Potential Program MRTN-CT-2004-005104. S.R. is supported by the EC's Marie Curie Research Training Network under the contract MRTN-CT-2004-512194 "Superstrings".

A Perfect matchings in the operator formalism

In Section 3.3, we found the loop states to be combinations of two perfect matchings. It would be interesting to recover the same result in terms of the operator formalism of Section 3.4. To do so, we start by distinguishing between even and odd plaquettes. We will say that a plaquette with coordinates $\mathbf{z} = (z, w)$ is *even* (resp. *odd*) if $z + w$ is even (resp. odd). We use the definition of the height function from the superposition of two perfect matchings $PM_1 - PM_2$ given in Section 2. If an odd plaquette contains either an upward arrow on the left side, a downward arrow on the right side, a right pointing arrow on the bottom side or a left pointing arrow on the upper side, it belongs to the first perfect matching PM_1 , in the converse case, it belongs to PM_2 . For an even plaquette, the arrows are reversed. The strategy to construct an operator which only preserves the operators corresponding to one of the perfect matchings, say PM_1 , when acting on a state $|\Psi\rangle$ is simple. Consider *e.g.* all the black nodes. For each of them add all the annihilators corresponding to the arrows belonging to PM_2 . If $|\Psi\rangle$ is an allowed state, only one operator is paired for each node which gives a 1 as a result of the anticommutation, while all the others will just annihilate the state. This results in only the operators belonging to PM_1 surviving and so yielding the result we are looking for. We can define the operators PM_1 and PM_2 explicitly as follows:

$$PM_1 = \prod_{z=1}^N \prod_{w=1}^M \frac{1 + (-1)^{z+w}}{2} [a(z, w) + d(z, w) + b(z, w - 1) + c(z - 1, w)] , \quad (108a)$$

$$PM_2 = \prod_{z=1}^z \prod_{w=1}^w \frac{1 + (-1)^{z+w}}{2} [b(z, w) + c(z, w) + a(z, w - 1) + d(z - 1, w)] . \quad (108b)$$

A state $|\Psi\rangle = |m_1\rangle \otimes |m_2\rangle$ is decomposed into its two constituent perfect matchings by their action:

$$PM_i |\Psi\rangle = |m_i\rangle, \quad i = 1, 2. \quad (109)$$

Now we are able to give a consistency condition for a state to correspond to a loop appearing in the expansion of the fermionic action. The idea is that the state should be decomposable into two matchings, which both touch each node once. Let us therefore define

$$P_1(z, w) = \frac{1+(-1)^{z+w}}{2} [N_a(z, w) + N_d(z, w) + N_b(z, w-1) + N_c(z-1, w) - 1], \quad (110a)$$

$$P_2(z, w) = \frac{1+(-1)^{z+w}}{2} [N_b(z, w) + N_c(z, w) + N_a(z, w-1) + N_d(z-1, w) - 1]. \quad (110b)$$

An allowed state $|\Psi\rangle$ must satisfy the local conditions

$$P_1(\mathbf{z}) |\Psi\rangle = P_2(\mathbf{z}) |\Psi\rangle = 0, \quad \forall \mathbf{z}. \quad (111)$$

The action of the height operators in Eq. (45) is still defined on the perfect matching states $|\Psi\rangle$. To be consistent with the constructions in Section 2, we introduce a sign to distinguish between $|m_1\rangle$ and $|m_2\rangle$:

$$H_z |m_i\rangle = (-1)^{i+1} \left[\sum_{\zeta=1}^N N_a(\zeta, \bar{w}) - N_b(\zeta, \bar{w}) \right] |m_i\rangle, \quad (112a)$$

$$H_w |m_i\rangle = (-1)^{i+1} \left[\sum_{\omega=1}^M N_c(\bar{z}, \omega) - N_d(\bar{z}, \omega) \right] |m_i\rangle. \quad (112b)$$

We find that each loop can be identified by four charges, corresponding to the eigenvalues of the winding operators acting on the two perfect matchings. The relation between the winding of a loop and the weights of the constituent perfect matchings is

$$H_z |\Psi\rangle = H_z |m_1\rangle - H_z |m_2\rangle, \quad (113a)$$

$$H_w |\Psi\rangle = H_w |m_1\rangle - H_w |m_2\rangle. \quad (113b)$$

Extending the definition of the height function to perfect matchings requires some care, since the equality in Eq. (43) does not hold for perfect matchings. A possible way out consists in symmetrizing the sum of the two expressions and define

$$h(z, w) |m_i\rangle = \frac{(-1)^{i+1}}{2} \left[\sum_{\zeta=0}^z N_a(\zeta, w) - N_b(\zeta, w) + \sum_{\omega=0}^w N_c(z, \omega) - N_d(z, \omega) \right] |m_i\rangle. \quad (114)$$

In this way, one recovers once more

$$h(\mathbf{z}) |\Psi\rangle = h(\mathbf{z}) |m_1\rangle - h(\mathbf{z}) |m_2\rangle. \quad (115)$$

B Generating functions

In this section, we give the generating function which contains the full information of the fermion loop gas, *i.e.* all the loop states. The dimer model partition function and the Witten index can be recovered from it.

B.1 Generating function for the fermion loops on the cylinder

We compute the generating functions for the loops defined as

$$G(q, z, y) = \text{Tr} \left[q^H z^K y^F \right], \quad (116)$$

which keeps track of all the information. Expanding the trace one finds an explicit expression depending on the matching degeneracies N_k :

$$G(q, z, y) = \sum_{k=0}^N N_k y^{2k} z^k + (1+y) \left\{ \frac{1}{2} \sum_{k=0}^N N_k (N_k - 1) y^{2k} z^k + \sum_{l=1}^N q^l \sum_{k=l}^N N_k N_{k-l} y^{2k} z^k \right\}. \quad (117)$$

All the physical information about the system is contained in the generating function G . For example:

- the Euler number for the complex in Eq. (64) is $\chi = \text{Tr} \left[(-1)^F \right] = G(1, 1, -1)$;
- the Poincaré polynomial for the complex is $\chi(z) = \text{Tr} \left[(-1)^F z^k \right] = G(1, z, -1)$;
- the total number of perfect matchings is $N = \text{Tr} \left[(-1)^{K+F} \right] = G(1, -1, -1)$;
- the multiplicity of weight- k matchings is $N_k = \frac{1}{k!} \frac{\partial^k}{\partial z^k} G(q, \frac{z}{y}, y) \Big|_{q=1, z=0, y=-1}$;
- the dimension of the k -th chain group is $\dim C_k = \frac{1}{k!} \frac{\partial^k}{\partial y^k} G(q, z, y) \Big|_{q=1, z=1, y=0}$;
- the number of loops with winding number h is $L_h = \frac{1}{h!} \frac{\partial^h}{\partial q^h} G(q, z, y) \Big|_{q=0, z=1, y=1}$.

B.2 Generating function for the fermion loops on the torus

Let us now extend the definition of generating function for the loops to graphs embedded on the torus. Following the formula for the cylinder in Eq. (117) we define:

$$G(\mathbf{q}, \mathbf{z}, y) = \text{Tr} \left[\mathbf{q}^H \mathbf{z}^K y^F \right], \quad (118)$$

where the notation $\mathbf{q}^{\mathbf{H}}$ is a shortcut for $\mathbf{q}^{\mathbf{H}} \doteq q_z^{H_z} q_w^{H_w}$ and $\mathbf{z}^{\mathbf{k}} \doteq z^{k_z} w^{k_w}$. Expanding in the loop basis we find:

$$G(\mathbf{q}, \mathbf{z}, y) = \sum_{\mathbf{k}=(0,0)}^{\mathbf{N}} N_{\mathbf{k}} y^{2k_z} \mathbf{z}^{\mathbf{k}} + \frac{1+y}{2} \left\{ \sum_{\mathbf{k}=(0,0)}^{\mathbf{N}} N_{\mathbf{k}} (N_{\mathbf{k}} - 1) y^{2k_z} \mathbf{z}^{\mathbf{k}} + \sum_{\mathbf{l}=(0,0)}^{\mathbf{N}} \mathbf{q}^{\mathbf{l}} \sum_{\mathbf{k}=\mathbf{l}}^{\mathbf{N}} \left(N_{\mathbf{k}} N_{\mathbf{k}-\mathbf{l}} + N_{k_z(k_w-l_w)} N_{(k_z-l_z)k_w} \right) y^{2k_z} \mathbf{z}^{\mathbf{k}} \right\}, \quad (119)$$

where the primed sum $\sum_{\mathbf{l}}'$ means that the value $\mathbf{l} = (0,0)$ is to be omitted. All the physics of the system is encoded into $G(\mathbf{q}, \mathbf{z}, y)$. In particular:

- the Euler number for the complex in Eq. (89) is $\chi(w) = \text{Tr} [(-1)^F w^{K_w}] = G((1,1), (1, w), -1)$;
- the Poincaré characteristic for the complex is $\chi(z, w) = \text{Tr} [(-1)^F \mathbf{z}^{\mathbf{k}}] = G((1,1), \mathbf{z}, -1)$;
- the number of perfect matchings with height \mathbf{k} is $N_{\mathbf{k}} = \frac{1}{\mathbf{k}!} \frac{\partial^{|\mathbf{k}|}}{\partial \mathbf{z}^{\mathbf{k}}} G \Big|_{\mathbf{q}=(1,1), \mathbf{z}=(0,0), y=-1}$, where we introduced the notation $\mathbf{k}! \doteq k_z! k_w!$, $|\mathbf{k}| \doteq k_z + k_w$, and $\frac{\partial^{|\mathbf{k}|}}{\partial \mathbf{z}^{\mathbf{k}}} \doteq \frac{\partial^{k_z+k_w}}{\partial z^{k_z} \partial w^{k_w}}$;
- the dimension of the $C_{\mathbf{k}}$ chain group is $\dim C_{\mathbf{k}} = \frac{1}{\mathbf{k}!} \frac{\partial^{|\mathbf{k}|}}{\partial y^{k_z} \partial w^{k_w}} G \Big|_{\mathbf{q}=(1,1), \mathbf{z}=(0,1), y=1}$;
- the number of loops with winding \mathbf{h} is $L_{\mathbf{h}} = \frac{1}{\mathbf{h}!} \frac{\partial^{|\mathbf{h}|}}{\partial \mathbf{q}^{\mathbf{h}}} G \Big|_{\mathbf{q}=(0,0), \mathbf{z}=(1,1), y=1}$.

C Example: One square on the torus

To illustrate the construction given in Section 4.4, we now present the smallest possible example on the torus, consisting only of one square. The eight possible matchings and their quantum numbers are shown in Figure 9. They combine into 64 loop configurations, which are, sorted into their co-chain groups according to total winding number, depicted in Table 4.

The partition function of the dimer model is the one given in (102), the generating function for this example reads

$$G(\mathbf{q}, \mathbf{z}, y) = w + y^2 z + 4wy^2 z + w^2 y^2 z + wy^4 z^2 + (1+y) \left[(6wy^2 z + 4q_z + 4q_w + q_z q_w) wy^2 z + (4q_w + q_w^2 + q_z q_w) w^2 y^2 z + (4q_z + q_z^2 + q_z q_w) wy^4 z^2 + q_z q_w w^2 y^4 z^2 \right]. \quad (120)$$

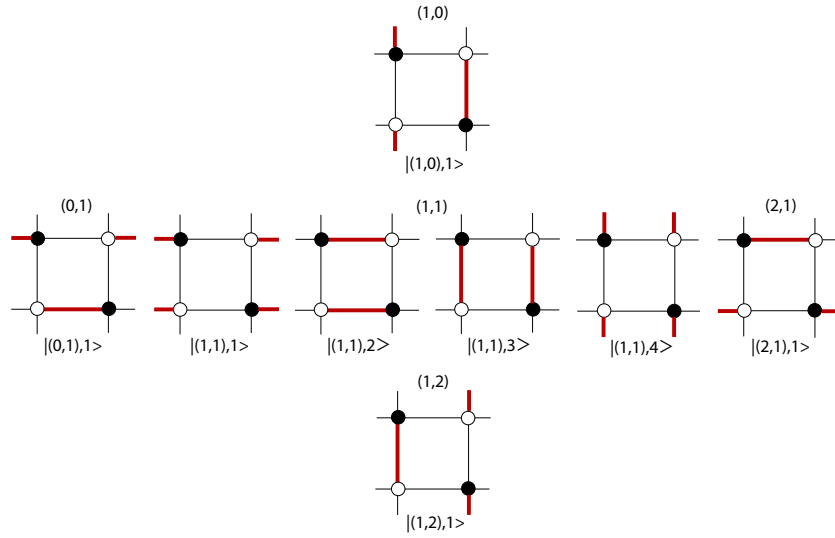


Figure 15: Matchings for the square on the torus

Table 4: Co-chain groups for the square on the torus

K_w	C^0	C^1	C^2	C^3	C^4	C^5
2	-	-	$ 1, 2, 1; 0, 1, 1\rangle_+$ 	$ 1, 2, 1; 0, 1, 1\rangle_-$ 	-	-
2	-	-	$ 1, 2, 1; 1, 0, 1\rangle_+$ 	$ 1, 2, 1; 1, 0, 1\rangle_-$ 	-	-
2	-	-	$ 1, 2, 1; 1, 1, 4\rangle_+$ 	$ 1, 2, 1; 1, 1, 4\rangle_-$ 	-	-
2	-	-	$ 1, 2, 1; 1, 1, 3\rangle_+$ 	$ 1, 2, 1; 1, 1, 3\rangle_-$ 	-	-
2	-	-	$ 1, 2, 1; 1, 1, 2\rangle_+$ 	$ 1, 2, 1; 1, 1, 2\rangle_-$ 	-	-

Continued on next page

Table 4 – continued from previous page

K_w	C^0	C^1	C^2	C^3	C^4	C^5
2	-	-	$ 1, 2, 1; 1, 1, 1\rangle_+$ 	$ 1, 2, 1; 1, 1, 1\rangle_-$ 	-	-
2	-	-	$ 1, 2, 1; 1, 2, 1\rangle$ 	-	$ 2, 1, 1; 1, 2, 1\rangle_+$ 	$ 2, 1, 1; 1, 2, 1\rangle_-$
1	-	-	$ 1, 1, 4; 0, 1, 1\rangle_+$ 	$ 1, 1, 4; 0, 1, 1\rangle_-$ 	-	-
1	-	-	$ 1, 1, 3; 0, 1, 1\rangle_+$ 	$ 1, 1, 3; 0, 1, 1\rangle_-$ 	-	-
1	-	-	$ 1, 1, 2; 0, 1, 1\rangle_+$ 	$ 1, 1, 2; 0, 1, 1\rangle_-$ 	-	-
1	-	-	$ 1, 1, 1; 0, 1, 1\rangle_+$ 	$ 1, 1, 1; 0, 1, 1\rangle_-$ 	-	-
1	-	-	$ 1, 0, 1; 0, 1, 1\rangle_+$ 	$ 1, 0, 1; 0, 1, 1\rangle_-$ 	-	-
1	-	-	$ 1, 1, 4; 1, 0, 1\rangle_+$ 	$ 1, 1, 4; 1, 0, 1\rangle_-$ 	-	-
1	-	-	$ 1, 1, 3; 1, 0, 1\rangle_+$ 	$ 1, 1, 3; 1, 0, 1\rangle_-$ 	-	-
1	-	-	$ 1, 1, 2; 1, 0, 1\rangle_+$ 	$ 1, 1, 2; 1, 0, 1\rangle_-$ 	-	-

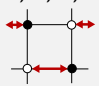
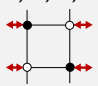
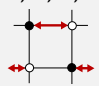
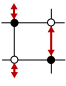
Continued on next page

Table 4 – continued from previous page

K_w	C^0	C^1	C^2	C^3	C^4	C^5
1	-	-	$ 1, 1, 1; 1, 0, 1\rangle_+$ 	$ 1, 1, 1; 1, 0, 1\rangle_-$ 	-	-
1	-	-	$ 1, 1, 4; 1, 1, 3\rangle_+$ 	$ 1, 1, 4; 1, 1, 3\rangle_-$ 	-	-
1	-	-	$ 1, 1, 4; 1, 1, 2\rangle_+$ 	$ 1, 1, 4; 1, 1, 2\rangle_-$ 	-	-
1	-	-	$ 1, 1, 4; 1, 1, 1\rangle_+$ 	$ 1, 1, 4; 1, 1, 1\rangle_-$ 	-	-
1	-	-	$ 1, 1, 3; 1, 1, 2\rangle_+$ 	$ 1, 1, 3; 1, 1, 2\rangle_-$ 	$ 2, 1, 1; 0, 1, 1\rangle_+$ 	$ 2, 1, 1; 0, 1, 1\rangle_-$
1	-	-	$ 1, 1, 3; 1, 1, 1\rangle_+$ 	$ 1, 1, 3; 1, 1, 1\rangle_-$ 	$ 2, 1, 1; 1, 0, 1\rangle_+$ 	$ 2, 1, 1; 1, 0, 1\rangle_-$
1	-	-	$ 1, 1, 2; 1, 1, 1\rangle_+$ 	$ 1, 1, 2; 1, 1, 1\rangle_-$ 	$ 2, 1, 1; 1, 1, 4\rangle_+$ 	$ 2, 1, 1; 1, 1, 4\rangle_-$
1	-	-	$ 1, 1, 4; 1, 1, 4\rangle$ 	-	$ 2, 1, 1; 1, 1, 3\rangle_+$ 	$ 2, 1, 1; 1, 1, 3\rangle_-$
1	-	-	$ 1, 1, 3; 1, 1, 3\rangle$ 	-	$ 2, 1, 1; 1, 1, 2\rangle_+$ 	$ 2, 1, 1; 1, 1, 2\rangle_-$
1	-	-	$ 1, 1, 2; 1, 1, 2\rangle$ 	-	$ 2, 1, 1; 1, 1, 1\rangle_+$ 	$ 2, 1, 1; 1, 1, 1\rangle_-$

Continued on next page

Table 4 – continued from previous page

K_w	C^0	C^1	C^2	C^3	C^4	C^5
1	$ 0, 1, 1; 0, 1, 1\rangle$ 	-	$ 1, 1, 1; 1, 1, 1\rangle$ 	-	$ 2, 1, 1; 2, 1, 1\rangle$ 	-
0	-	-	$ 1, 0, 1; 1, 0, 1\rangle$ 	-	-	-

References

- [1] P. Kasteleyn, *Dimer statistics and phase transitions*, *Journal of Mathematical Physics* **4** (1963) 287–293.
- [2] P. Kasteleyn, *The statistics of dimers on a lattice*, *Physica* **27** (1961) 1209–1225.
- [3] M. E. Fisher and H. N. V. Temperley, *Association problem in statistical mechanics—Critique of the treatment of H.S.Green and R.Leipnik*, *Rev. Mod. Phys.* **32** (Oct, 1960) 1029–1031.
- [4] M. E. Fisher, *Statistical mechanics of dimers on a plane lattice*, *Phys. Rev.* **124** (1961), no. 4 1664–1672.
- [5] C. Hurst and H. Green, *New solution to the Ising problem for a rectangular lattice*, *Journal of Chemical Physics* **33** (1960) 1059–1062.
- [6] R. Kenyon, *An introduction to the dimer model*, math.CO/0310326.
- [7] H. Cohn, R. Kenyon, and J. Propp, *A variational principle for domino tilings*, *J.Amer.Math.Soc.* **14** (2001), no. 2 297–346.
- [8] A. Okounkov, N. Reshetikhin, and C. Vafa, *Quantum Calabi-Yau and classical crystals*, hep-th/0309208.
- [9] A. Iqbal, N. Nekrasov, A. Okounkov, and C. Vafa, *Quantum foam and topological strings*, hep-th/0312022.
- [10] R. Kenyon and A. Okounkov, *Planar dimers and Harnack curves*, *Duke Math.J.* **131** (2006), no. 3 499–524, [math.AG/0311062].

- [11] R. Kenyon, A. Okounkov, and S. Sheffield, *Dimers and amoebae*, *Ann. of Math. (2)* **163** (2006), no. 3 1019–1056, [math-ph/0311005].
- [12] J. J. Heckman and C. Vafa, *Crystal melting and black holes*, hep-th/0610005.
- [13] A. Hanany and K. D. Kennaway, *Dimer models and toric diagrams*, hep-th/0503149.
- [14] S. Franco, A. Hanany, K. D. Kennaway, D. Vegh, and B. Wecht, *Brane dimers and quiver gauge theories*, *JHEP* **01** (2006) 096, [hep-th/0504110].
- [15] S. Franco *et. al.*, *Gauge theories from toric geometry and brane tilings*, *JHEP* **01** (2006) 128, [hep-th/0505211].
- [16] A. Hanany and D. Vegh, *Quivers, tilings, branes and rhombi*, hep-th/0511063.
- [17] A. Hanany, C. P. Herzog, and D. Vegh, *Brane tilings and exceptional collections*, *JHEP* **07** (2006) 001, [hep-th/0602041].
- [18] B. Feng, Y.-H. He, K. D. Kennaway, and C. Vafa, *Dimer models from mirror symmetry and quivering amoebae*, hep-th/0511287.
- [19] D. Cimasoni and N. Reshetikhin, *Dimers on surface graphs and spin structures. I*, math-ph/0608070.
- [20] M. Karowski, R. Schrader, and H. Thun, *Monte Carlo simulations for quantum field theories involving fermions*, *Commun.Math.Phys.* **97** (1985) 5–29.
- [21] M. Khovanov, *A categorification of the Jones polynomial*, *Duke Math. J.* **101** (2000), no. 3 359–426, [math.QA/9908171].
- [22] M. Khovanov, *Categorifications of the colored Jones polynomial*, *J. Knot theory and its Ramifications* **14** (2005), no. 1 111–130, [math.QA/0302060].
- [23] M. Khovanov, *Link homology and categorification*, *Proceedings of the ICM-2006, Madrid* **2** (2005) 989–999, [math.QA/0605339].
- [24] E. Caianiello, *Combinatorics and Renormalization in Quantum Field Theory*. Frontiers in Physics. W.A. Benjamin, Inc., Reading, Massachusetts, 1973.
- [25] L. Valiant, *The complexity of computing the permanent*, *Theoret. Comput. Sci.* **8** (1979) 189–201.
- [26] G. Kuperberg, *Symmetries of plane partitions and the permanent-determinant method*, *J. Combin. Theory Ser. A* **68** (1994), no. 1 115–151, [math.CO/9410224].
- [27] G. Polya, *Aufgabe 424*, *Arch. Math. Phys.* **20** (1913) 271.

- [28] G. Kuperberg, *An exploration of the permanent-determinant method*, *Electron. J. Combin.* **5** (1998), no. 1 R46, [math.CO/9810091].
- [29] E. H. Lieb, *Solution of the dimer problem by the transfer matrix method*, *Journal of Mathematical Physics* **8** (1967), no. 12 2339–2341.
- [30] B. Sutherland, *Correlation functions for two-dimensional ferroelectrics*, *Phys. Lett.* **A26** (1968), no. 11 532–533.
- [31] F. Alet, Y. Ikhlef, J. L. Jacobsen, G. Misguich, and V. Pasquier, *Classical dimers with aligning interactions on the square lattice*, *Physical Review E (Statistical, Nonlinear, and Soft Matter Physics)* **74** (2006), no. 4 041124.
- [32] R. Kenyon, *The Laplacian and Dirac operators on critical planar graphs*, *Invent. Math.* **150** (2002), no. 2 409–439, [math-ph/0202018].
- [33] J. M. Rabin, *Homology theory of lattice fermion doubling*, *Nucl. Phys.* **B201** (1982) 315.
- [34] P. Becher and H. Joos, *The Dirac-Kähler equation and fermions on the lattice*, *Zeit. Phys.* **C15** (1982) 343.
- [35] L. Susskind, *Lattice fermions*, *Phys. Rev. D* **16** (Nov, 1977) 3031–3039.
- [36] C. Nash and D. O’Connor, *Modular invariance, lattice field theories, and finite size corrections*, *Annals Phys.* **273** (1999) 72–98, [hep-th/9606137].
- [37] C. Nash and D. O’Connor, *Modular invariance of finite size corrections and a vortex critical phase*, *Phys. Rev. Lett.* **76** (1996) 1196–1199, [hep-th/9506062].
- [38] D. B. Ray and I. M. Singer, *Analytic torsion for complex manifolds*, *Annals Math.* **98** (1973) 154–177.
- [39] A. Ferdinand, *Statistical mechanics of dimers on a quadratic lattice*, *J. Math. Phys.* **8** (1967) 2332–2339.
- [40] A. E. Ferdinand and M. E. Fisher, *Bounded and inhomogeneous Ising models. I. Specific-heat anomaly of a finite lattice*, *Phys. Rev.* **185** (Sep, 1969) 832–846.
- [41] H. B. Nielsen and M. Ninomiya, *No go theorem for regularizing chiral fermions*, *Phys. Lett.* **B105** (1981) 219.
- [42] H. B. Nielsen and M. Ninomiya, *Absence of neutrinos on a lattice. 1. proof by homotopy theory*, *Nucl. Phys.* **B185** (1981) 20.
- [43] L. Helme-Guizon and Y. Rong, *A categorification for the chromatic polynomial*, *Alg. Geom. Top.* **5** (2005) 1365–1388.

- [44] L. Helme-Guizon and Y. Rong, *Graph homologies from arbitrary algebras*, math.QA/0506023.
- [45] E. F. Jasso-Hernandez and Y. Rong, *A categorification for the Tutte polynomial*, math.CO/0512613.
- [46] J. Baez and J. Dolan, *Higher Category Theory*, vol. 230 of *Contemp. Math.*, ch. Categorification, pp. 1–36. American Mathematical Society, Providence, Rhode Island, 1998. math.QA/9802029.
- [47] K. Hori, S. Katz, A. Klemm, R. Pandharipande, R. Thomas, C. Vafa, R. Vakil, and E. Zaslow, *Mirror Symmetry*. No. 1 in Clay Mathematics Monographs. American Mathematical Society, Clay Mathematics Institute, 2003.
- [48] P. S. Aspinwall, *D-branes on Calabi-Yau manifolds*, hep-th/0403166.
- [49] P. S. Aspinwall and I. V. Melnikov, *D-branes on vanishing del Pezzo surfaces*, *JHEP* **12** (2004) 042, [hep-th/0405134].
- [50] A. Rudakov, *Helices and Vector Bundles: Seminaire Rudakov*. No. 148 in London Mathematical Society Lecture Note Series. Cambridge University Press, Cambridge, 1990.
- [51] E. Zaslow, *Solitons and helices: The search for a math physics bridge*, *Commun. Math. Phys.* **175** (1996) 337–376, [hep-th/9408133].
- [52] R. M. Karp, *Reducibility among combinatorial problems.*, in *Complexity of Computer Computations* (R. Miller and J. Thatcher, eds.), pp. 85–103, Plenum, New York, 1972.
- [53] N. Seiberg, *Electric - magnetic duality in supersymmetric nonabelian gauge theories*, *Nucl. Phys.* **B435** (1995) 129–146, [hep-th/9411149].
- [54] F. Cachazo, B. Fiol, K. A. Intriligator, S. Katz, and C. Vafa, *A geometric unification of dualities*, *Nucl. Phys.* **B628** (2002) 3–78, [hep-th/0110028].
- [55] C. P. Herzog, *Seiberg duality is an exceptional mutation*, *JHEP* **08** (2004) 064, [hep-th/0405118].
- [56] Y.-H. He, *Lectures on D-branes, gauge theories and Calabi-Yau singularities*, hep-th/0408142.
- [57] C. P. Herzog, *Exceptional collections and del Pezzo gauge theories*, *JHEP* **04** (2004) 069, [hep-th/0310262].